Materials Advances

ROYAL SOCIETY OF CHEMISTRY

PAPER

View Article Online
View Journal | View Issue

Cite this: *Mater. Adv.*, 2025, 6, 682

Green synthesis of biocompatible silver nanoparticles using *Trillium govanianum* rhizome extract: comprehensive biological evaluation and *in silico* analysis†

Syed Ifrah Manzoor,[a] Farhat Jabeen,[a] Rajan Patel,[b] M. Moshahid Alam Rizvi,[c] Khalid Imtiyaz,[c] Maqsood Ahmad Malik *[d] and Tanveer A. Dar *[a]

Green synthesis of silver nanoparticles (AgNPs), using medicinal plants, is widely practiced due to the diverse bioactive compounds present in these plants, which can act synergistically with the AgNPs. Notably, the rhizome of *Trillium govanianum* Wall Ex. Royle is rich in bioactive phytochemicals such as steroids, saponins, glycosides, and fatty acids. This study aims to synthesize and characterize AgNPs mediated by the *Trillium govanianum* rhizome (^{TGR}AgNPs) and comprehensively investigate their biological activities. The results indicated that phytochemicals in the rhizome may function as reducing and capping agents in the synthesis of ^{TGR}AgNPs. Overall, this study presents a simple, rapid, cost-effective, and eco-friendly method for nanoparticle production. Subsequently, the ^{TGR}AgNPs were characterized using UV-vis spectroscopy, FTIR, XRD, DLS, zeta potential, SEM-EDX, and TEM analyses. GC-MS analysis of the extract identified several phytochemicals that might play crucial role in the synthesis of ^{TGR}AgNPs. Moreover, ^{TGR}AgNPs demonstrated significant antioxidant, anticancer (against HCT-116 cell lines), anti-inflammatory, and DNA protection activities. Additionally, hemolytic assay confirmed the non-toxic and hemo-compatible nature of ^{TGR}AgNPs at all tested concentrations. The findings suggest that the green synthesized ^{TGR}AgNPs have promising potential as biocompatible antioxidant, anti-inflammatory, and anticancer agents in biomedicine.

Received 23rd September 2024,
Accepted 3rd December 2024

DOI: 10.1039/d4ma00959b

rsc.li/materials-advances

1. Introduction

Nanoscience is rapidly emerging as a pivotal field for producing various metal nanoparticles, which have diverse applications in biomedicine and diagnostics.[1,2] Due to their unique physicochemical properties, these metal nanoparticles hold great promise in biotechnology, biomedicine, optoelectronics, diagnostics, therapy, and bio-sensing.[3,4] Silver nanoparticles (AgNPs) have garnered significant attention for their exceptional biocompatibility, low toxicity, and multiple biological activities, including antimicrobial, anticancer, and antioxidant effects.[5,6] Consequently, the synthesis of AgNPs has become a focal point for the scientific community. Several physicochemical methods, such as gamma-ray radiation, autoclaving, electrochemical techniques, and chemical reduction approaches, are being explored to achieve efficient yields of AgNPs.[7] However, these methods are often expensive, time-consuming, energy-intensive, and require extreme experimental conditions like high temperatures, pressures, and sophisticated equipment. The adverse effects of toxic agents adsorbed and capped on nanoparticle surfaces remain a significant concern.[8,9] Conversely, biological approaches using bio-resources such as plants and microorganisms are becoming increasingly popular for synthesizing AgNPs with biomedical applications. These methods are cost-effective, less time-consuming, have reduced toxicity, and are more sustainable compared to traditional physicochemical techniques.[10–12] Furthermore, these biological agents are inherently biocompatible and biodegradable, allowing for simple scale-up to large-scale production.[13] Generally, for a process to be suitable for its scale-up to industrial level, a number of criteria need to be satisfied such as – (i) the raw materials, products, by-products, and wastes must be environmentally friendly, (ii) the required raw material should be producible, industrially abundant, and available in large scale, (iii) the conditions required for the process should be well defined with an ability to be controlled

[a] *Department of Clinical Biochemistry, University of Kashmir, Srinagar-190006, Jammu and Kashmir, India. E-mail: tanveerali@kashmiruniversity.ac.in*
[b] *Centre for Interdisciplinary Research in Basic Sciences, Jamia Millia Islamia, New Delhi-110025, India*
[c] *Department of Biosciences, Faculty of Life Sciences, Jamia Millia Islamia, New Delhi-110025, India*
[d] *Department of Chemistry, Faculty of Sciences, Jamia Millia Islamia, New Delhi-110025, India. E-mail: mamalik@jmi.ac.in*

† Electronic supplementary information (ESI) available. See DOI: https://doi.org/10.1039/d4ma00959b

automatically and (iv) the production process should be economically appropriate for investment. In light of these, green synthesized nanoparticles are emerging as potential candidates for large-scale nanoparticle production. Among the synthesizing agents, plant extracts are particularly advantageous for the green synthesis of AgNPs as the phytochemical constituents in the extracts prevent nanoparticle aggregation and efficiently reduce metal precursors, resulting in the rapid formation of stable nanoparticles.[14–16] More importantly, the coated bioactive phytochemical constituents exhibit synergistic effects with the synthesized AgNPs. Due to this, traditional Indian medicinal herbs have attracted increased attention for their use in nanoparticle synthesis.[17–21]

To date, several Indian medicinal herbs such as *Ocimum tenuiflorum*,[22] *Lysinibacillus fusiformis*,[23] *Azadirachta indica*,[24] *ficus bengalensis*,[25] *ocimum sanctum*,[26] *Tridax procumbens*[27] *etc.*, have been employed in green fabrication of AgNPs with significant biocompatibility and multifarious biological activities such as antioxidant, anti-inflammatory, cytotoxicity and DNA protection. In addition to this, *Solanum trilobatum, Indoneesiella echioides, Azadirachta indica and Achillea biebersteinii*-mediated AgNPs exhibit potent biological activities, including antimicrobial, antioxidant, and cytotoxicity.[28–31] Furthermore, *P. fulges*-mediated AgNPs showed effective cytotoxicity against various cell lines, while banana peel extract-mediated synthesized nanoparticles exhibit potent antibacterial properties.[32] *Trillium govanianum* Wall. ex D. Don, native to high-altitude ranges of the Himalayas, is also a high-value medicinal plant from the family Melanthiacea. Morphologically, *Trillium govanianum* is a small herb characterized by three ovate leaves and a distinct stalk. It is abundant in bioactive phytochemicals, including fatty acids, phenols, hydrocarbons, saponins, carbohydrates, and steroids, contributing to its diverse biological activities.[33] Among different parts of the plant, rhizomes have garnered significant attention due to the rich content of potent bioactive compounds such as diosgenin and glycosides, which are widely utilized in preparing steroidal and sex hormones. So far, only a single study has reported on *Trillium govanianum*-mediated AgNPs with antimicrobial properties.[34] The present investigation marks the first comprehensive exploration of a simple, sustainable, rapid and cost-effective method for the green synthesis of highly biocompatible AgNPs, utilizing aqueous extract from *Trillium govanianum* rhizomes. Additionally, we conducted a detailed evaluation of the green synthesized biocompatible AgNPs for various biological activities such as antioxidant, anti-inflammatory, cytotoxicity and DNA damage protection. Moreover, *in silico* analysis was carried out to identify possible target molecules and pathways implicated in the biological activities of the synthesized silver nanoparticles.

2. Experimental

2.1. Materials

Silver nitrate ($AgNO_3$, 99.5% purity), 1,1-diphenyl-2-picrylhydrazyl (DPPH), (3-[4,5-dimethylthiazol-2-yl]-2,5 diphenyl tetrazolium bromide (MTT), L-Ascorbic acid (99% purity), and methanol were purchased from Sigma Aldrich, USA. *Trillium govanianum* rhizome leaves were collected from the higher reaches of the Kashmir Himalayas. All other chemicals were of analytical grade with highest purity and were used without any additional purification.

2.2. Preparation and phytochemical analysis of *T. govanianum* rhizome extract

The aqueous extract of *T. govanianum* was prepared by dissolving 5 mg of the extract in 10 mL of distilled water. To remove the debris/impurities, the aqueous extract was filtered through standard filter paper followed by Whatman filter paper No. 1. The filtered solution, referred here as *Trillium govanianum* rhizome (TGR) extract, was used as a reducing and stabilizing agent for the nanoparticle synthesis. Subsequently, Gas chromatography – Mass spectrometry (GC-MS) analysis of the TGR extract was performed using Agilent 7000 D triple quadrupole GC/MSD. Helium was used as the carrier gas at a flow rate of 1 mL min^{-1}. A 1 : 100 v/v sample dilution in hexane was made, and 1.0 μL of sample was injected. The temperature of the column was first adjusted to 50 °C. It was then progressively raised to 150 °C at a 3 °C min^{-1} rate and eventually raised to 250 °C at 10 °C min^{-1}. The electron emission and ionization energy were 100 μA and 70 eV, respectively. The inbuilt NIST library of the GC-MS instrument was used to establish the structure, name, and molecular structure of the phytochemicals of TGR extract.

2.3. Synthesis of *Trillium govanianum*-mediated AgNPs (^{TGR}AgNPs)

For the preparation of ^{TGR}AgNPs, 50 mL of 0.1 M silver nitrate aqueous solution was taken in a 250 mL beaker with constant stirring at 30 °C. To this solution, 50 mL of TGR extract was added and stirred for 15 minutes. Initially, the formation of ^{TGR}AgNPs was observed by a colour change from yellowish to dark brown, followed by its confirmation through UV-visible spectra measurements at different time intervals and days. The prepared ^{TGR}AgNPs were collected as pellets after centrifugation at 10 000 rpm for 20 minutes, followed by several washings with deionized water and ethanol to remove unreacted material or impurities. The final green synthesized ^{TGR}AgNPs were dried at 60 °C for 24 h and stored in a dark glass bottle at 4 °C for further characterization and activity studies.

2.4. Characterization of ^{TGR}AgNPs

The bioreduction of silver ions to silver nanoparticles was characterized by monitoring its UV-vis spectra using Cary-100 UV-visible spectrophotometer at wavelength range of 200–800 nm. The spectra were taken at different time intervals to confirm the complete reduction of Ag^+ to Ag^0. To assess the stability of the nanoparticles, the spectra were taken over a period of 5 days and at different temperatures. The functional groups responsible for capping/stabilizing the AgNPs and the phytochemical constituents of the plant extract were identified by FTIR (Fourier transform infrared) spectroscopy. The FTIR spectra were collected using the Burker Tensor 37 instrument.

All the spectroscopic measurements were taken in 450–4000 cm^{-1} range. Scanning electron microscopy (SEM) was performed to confirm the surface morphology of the nanoparticle. For this study, a thin layer of the ^{TGR}AgNPs was placed on a carbon-coated copper grid. The grid was kept under a mercury lamp for 5 minutes to allow the sample to completely dry and the images were recorded. Furthermore, the size, shape and the corresponding selected area electron diffraction (SAED) were analysed with a transmission electron microscope (TEM). SAED is a two-dimensional electron diffraction pattern used to study the lattice parameters and crystallinity of materials. The samples for TEM analysis were prepared by dissolving the ^{TGR}AgNPs in distilled water. The sample was sonicated for 5 minutes, placed on the copper grid, and dried. The images were recorded at different magnification powers. The X-ray diffraction (XRD) technique was employed to ascertain the crystal structure of ^{TGR}AgNPs by examining the location and intensities of diffraction peaks, commonly observed in highly crystalline substances. The diffraction pattern was captured within a range of diffraction angles spanning from 20° to 80°. The XRD investigations were performed with a D8 Advance, Bruker, Germany X-ray diffractometer with Cu Kα (1.542 Å) radiation source. Dynamic light scattering (DLS) approach was employed to assess the hydrodynamic particle size distribution, polydispersity index (PDI), and ζ-potential of the nanoparticles using a Zetasizer nano ZS equipment (Malvern Instruments, Malvern, U.K.). The light scattering angle was set at 90°, and the size measurements were performed at 25 °C. The electrophoretic cell was utilized to measure the surface charge, also known as the ζ-potential, of the ^{TGR}AgNPs in an electric field. The preparation of the sample mainly involved the dilution of the nanoparticles with MilliQ water and subjecting them to ultrasonication for 5 minutes, resulting in the formation of a uniformly disseminated suspension.

2.5. Free radical scavenging activity

For assessing the antioxidant activity of the ^{TGR}AgNPs, the DPPH assay was performed as per the established method[35] with slight modifications. Different concentrations of ^{TGR}AgNPs (0.05, 0.1, 0.15, 0.2, and 0.25 mg mL^{-1}) were added to 1 mL of DPPH (0.02 mg mL^{-1}), with vigorous shaking followed by incubation at room temperature for 30 minutes. Ascorbic acid was used as a positive control, and methanol as a blank. The absorbance was measured at 515 nm and analyzed using a Cary 300 UV-vis spectrophotometer. The percentage scavenging activity was calculated by the following equation:

$$\text{Scavenging activity}(\%) = \frac{(A_c - A_s)}{A_c} \times 100 \quad (1)$$

where A_c is the absorbance of the control and A_s is the absorbance of the sample. All the experiments were performed in triplicate.

2.6. Hemo-compatibility assay

Compatibility of ^{TGR}AgNPs for red blood cells (RBCs) was observed using a haemolytic assay as per the already established protocol,[36] with slight modifications. Briefly, fresh blood samples (5 mL) were collected from healthy volunteers at the Diagnostic Centre of the Department of Clinical Biochemistry, University of Kashmir, in EDTA tubes. The blood samples were centrifuged at 2000 rpm for 15 minutes at 4 °C to separate the cells from the serum. After separation from the serum, the precipitated RBCs were washed thrice in PBS buffer (pH 7.4). RBC_S were dispersed in PBS to prepare RBC suspension (1%). Following this, 1 mL of RBC suspension in separate tubes was mixed with different concentrations of ^{TGR}AgNPs (0.05, 0.1, 0.2, 0.5, and 1 mg mL^{-1}). Following incubation at 37 °C, the tubes were centrifuged at 800 g for 5 minutes. The supernatant formed was collected, and measured its absorbance at 545 nm. RBCs were treated with phosphate-buffered saline (PBS) and Triton-X as negative and positive controls, respectively. All the experiments were done in triplicates. The percentage of haemolysis was calculated by the following formula:

$$\%\,\text{Haemolysis} = \frac{(A_t - A_n)}{(A_c - A_n)} \times 100 \quad (2)$$

where A_t represents the absorbance of the test sample, A_n is the absorbance of the negative control, and A_c is the absorbance of the positive control.

2.7. Cytotoxic activity assay

Cytotoxic effect of ^{TGR}AgNPs was performed on the HCT-116 cell line under *in vitro* conditions, using standard MTT assay.[37] The cell lines were obtained from the National Centre for Cell Science, Pune, India. In this assay, HCT-116 cells were plated in a 96-well plate at a density of 1×10^4 cells per well and allowed to attach overnight. After removing the supernatant, different concentrations of ^{TGR}AgNPs (0.05–0.5 mg mL^{-1}) were added to each well, and the cells were allowed to grow at 37 °C with 5% CO_2 for 24 h. Following this, MTT was added to each well, and plates were kept at 37 °C for 4 h. After 4 h, MTT was replaced with 200 μL DMSO, and cells were agitated for 5 minutes. Absorbance at 570 nm was measured using an iMark Microplate reader (Biorad, USA). Absorbance measured was used to calculate the percentage of cell cytotoxicity using the formula:

$$\text{Cell cytotoxicity}\,(\%) = \frac{(A_c - A_s)}{A_c} \times 100 \quad (3)$$

where A_s is the absorbance of the treated sample and A_c is the absorbance of the control.

2.8. Anti-inflammatory activity

In vitro anti-inflammatory activity of ^{TGR}AgNPs was carried out as per the already established protocol[38] with some minor modifications. Briefly, the reaction mixture consisted of 2.8 mL of PBS, 0.2 mL of 5% Bovine Serum Albumin (BSA), and different volumes of the ^{TGR}AgNPs with a concentration range of 0.1–0.4 mg mL^{-1}. The total volume was made up to 5 mL using PBS. The mixture was then incubated at 37 °C for 20 minutes and then at 70 °C for 10 minutes. After cooling, the absorbance of the mixture was monitored at 660 nm. The solution of PBS (2.8 mL) and BSA (0.2 mL) was used as control,

and diclofenac sodium was taken as a standard. The following equation was used to calculate the inhibition percentage of protein denaturation.

$$\text{Inhibition}(\%) = \frac{(A_c - A_s)}{A_c} \times 100 \quad (4)$$

where A_c indicates absorbance of the control, and A_s is the absorbance of the sample.

2.9. DNA damage protection assay

The DNA damage protection potential of ^{TGR}AgNPs was evaluated by DNA nick assay as described earlier[39] with minor modifications. In this, a mixture of 20 μL of calf thymus DNA and 1 μL of different concentrations of ^{TGR}AgNPs (0.1–0.9 mg mL^{-1}) were added to 3 μL of Fenton's reagent (30 mM H_2O_2, 100 mM ascorbic acid and 20 mM ferric nitrate). The reaction mixture was then incubated at 37 °C for 20 minutes. Post incubation, 3 μL of orange G dye (6×) was added to the mixture. Following this, the reaction mixture was loaded on 1% agarose gel, and electrophoresis was run for 10 minutes at 155 V, followed by ethidium bromide staining. Observed bands were visualized using an imager gel documentation system (Benchtop UV Transilluminator).

2.10. Experimental and statistical analysis

All the experiments were conducted in triplicate and One-Way ANOVA with Bonferroni *t*-test was applied to analyse intergroup differences and the results obtained were presented either as mean value ± standard deviation or the corresponding percentage error, wherever applicable, with respective p values as indicated in the respective result sections. The spectra and profiles displayed are indicative of a minimum of three separate measurements for each concentration.

3. Network pharmacology-based analysis

3.1. Physicochemical parameters of palmitic acid

The SMILES notation for palmitic acid was provided as input to SwissADME, a publicly accessible online tool (**https://www.swissadme.ch/**), designed for rapid and robust prediction of physicochemical characteristics and pharmacokinetic parameters, including ADME (Absorption, Distribution, Metabolism, and Excretion) properties. SwissADME employs state-of-the-art computational methodologies to efficiently compute drug-likeness (DL), oral bioavailability (OB), Caco-2 permeability, lipophilicity, and other relevant features for naturally occurring small molecules. The evaluation of the compound's drug-likeness was determined in accordance with Lipinski's rules and other guidelines.[40]

3.2. Identification of palmitic acid target genes

In this, the saturated data file (SDF), containing the chemical structure of palmitic acid, was acquired from the PubChem database (**https://pubchem.ncbi.nlm.nih.gov**). Subsequently was imported to two separate web-based server databases, PharmMapper (**https://lilab.ecust.edu.cn/pharmmapper/**)[41] and SwissTarget[42] for identification of its related target genes. The list of potential target genes was then retrieved as a CSV file, and the gene names were standardized to gene symbols by consulting the UniProt database (**https://www.uniprot.org**).

3.3. Protein–protein interaction (PPI) network construction

The PPI network is a pictorial representation of the highly specific protein–protein edge interaction for the identification of key genes and potential biomarkers involved in several biological processes. For this, the Network Analyst free web tool, STRING, was used to construct the PPI network based on the physical connections between the palmitic acid gene targets.[43,44] A minimum cutoff confidence score of 0.70 was used to develop the network, and the output data was analysed using cytoscape 3.8.2.

3.4. Gene ontology (GO) and pathway enrichment analysis

For this, functional analysis was carried out to evaluate the biological activities of the palmitic acid gene targets through GO and pathway analysis by using Shiny GO.[45] Generally, GO is a powerful computational tool for performing enrichment analysis on gene sets wherein the GO terms and pathways are primarily grouped into three biological functions *i.e.*, biological process (BP), Cellular component (CC) and Molecular function (MF).[46] The pathway-related data was extracted using the Kyoto Encyclopedia of Genes and Genomes (KEGG) database. KEGG pathway is a collection of pathway maps used to understand the high-level functioning of biological processes, including metabolism, human diseases and drug development.

Ethical statement. All the experiments were performed in compliance with the relevant laws and Institutional guidelines as per the Institutional Biosafety Committee, University of Kashmir.

4. Results and discussion

Developing reliable and eco-friendly approaches for generating biologically active nanoparticles is an emerging area of research in nanotechnology. Generally, green synthesis employs environmental friendly natural materials, instead of chemicals, for nanoparticle synthesis. Among these, plant-based extracts have been widely utilized to synthesize different NPs with defined size, shape, and composition. Indeed, these extracts contain several classes of phytochemicals such as polyphenols, alkaloids, saponins, *etc.* that carry out reduction of metal.[47] Moreover, plant synthesized NPs, as compared to chemically synthesized ones, exhibit multifarious biological activities with least side effects. In light of this, the present study employed *Trillium govanianum* rhizome aqueous extract for green synthesis of silver nanoparticles, termed *Trillium govanianum*-silver nanoparticles (^{TGR}AgNPs), followed by their characterization and evaluation of several biological activities.

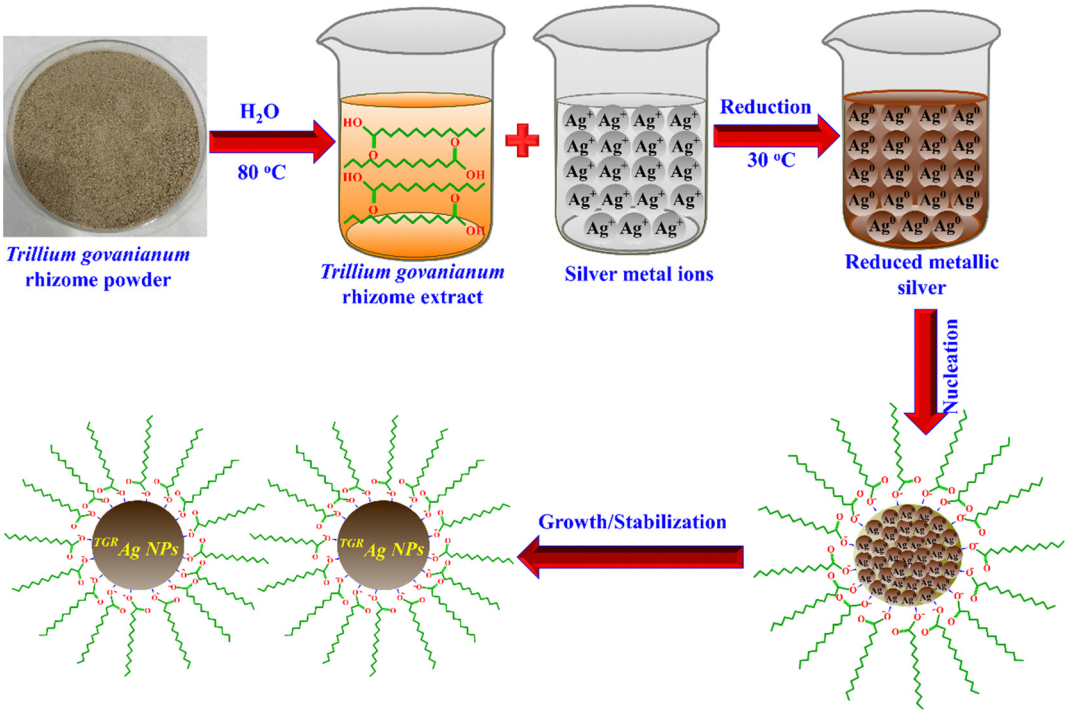

Fig. 1 Schematic illustration of *Trillium govanianum* rhizome extract mediated green synthesis of ^{TGR}AgNPs.

4.1. Synthesis of Ag NPs and GC-MS analysis of TGR extract

Generally, the synthesis of nanoparticles is ascertained by the visual colour change from pale yellow to brown. In light of this, 50 mL of 0.1 M $AgNO_3$ solution (Ag^+) was incubated with 50 mL of TGR extract (5 mg mL^{-1}), gradually changing the solution colour from pale yellow to dark brown within 15 minutes. Colour change, with time-dependent darkness of the brown colour, implies the reduction of Ag^+ to Ag^0 and resulting in the synthesis of ^{TGR}AgNPs. Post few hours, no change in colour intensity was observed, indicating complete reduction of silver ions in the reaction mixture. It is reported that the appearance of dark brown colour is due to the surface plasmon resonance (SPR) of AgNPs, regarded as an optical property of AgNPs.[48] Fig. 1 illustrates the schematic representation of the synthesis of ^{TGR}AgNPs as well as the observed change in solution colour.

The phytochemical components present in the methanolic rhizome extract of *T. govanianum* were further identified by GC-MS analysis. After careful analysis of the GC-MS chromatogram (Fig. S1, ESI†), the chemical profile of the rhizome extract and percent amount of the individual components obtained are summarized in Table S1 (ESI†). As can be seen from the results, GC-MS analysis of the TGR extract indicated presence of different classes of phytochemicals such as fatty acid esters, alkaloids, phenols, saponins, carbohydrates, and steroids (Table S1, ESI†). As can be seen from the results, 28 major compounds were identified in the methanolic extract of *T. govanianum* rhizome with corresponding significant peaks observed in the GC-MS chromatogram (Fig. S1, ESI†). Altogether, the dominant phytochemicals mainly included n-hexadecanoic acid (100%), 9,12-octadecanoic acid methyl ester (67.5), palmitoleic acid (45.7), 9,12-octadecadienoic acid (29%), alpha tocopherol-beta-D-mannoside (35.3%), hexadecanoic acid, 2-hydroxy-1-ethyl ester (20.4%), 9-octadecadienoic acid, methyl ester (20.15%), 11,14,17-eicosatrienoic acid (18%), diosgenin (17%), methyl hexadec-9-enoate (13%) and triacontane (10%). Interestingly, hexadecanoic acid (palmitic acid) and 9,12-Octadecadienoic acid (linoleic acid), observed as major constituents of our extract, have been reported to exhibit anticancer activity.[33,49] Moreover, diosgenin is reported to exhibit hypoglycaemic, hypolipidemic, antioxidant, anti-inflammatory, and antiproliferative activities while as tocopherol and astaxanthin are reported to have antioxidant properties.[50,51] As observed in our results, similar other studies have also reported the presence of n-hexadecanoic acid methyl ester, n-hexadecanoic acid, 9,12-octadecadienoic acid (Z, Z) and octadecanoic acid in the methanolic rhizome extract of *trillium govanianum*.[52]

It is a well-established fact that these phytochemicals contribute towards the reduction of Ag^+ by donating the electrons, transforming them into a large number of silver nuclei or zero-valent (Ag^0) atoms (Fig. 2).[53] The bioreduction process involves three main stages: activation, nucleation and growth. The reduction of Ag^+ ions occur in the activation stage which is followed by the nucleation of the reduced Ag atoms. During the growth stage, the spontaneous coalescence of small AgNPs into large-sized AgNPs takes place. In this final stage, where the AgNPs attain their ultimate shape, there is an increase in their thermodynamic stability, a process known as Ostwald ripening. It has been shown that phytochemicals act as stabilizing agents

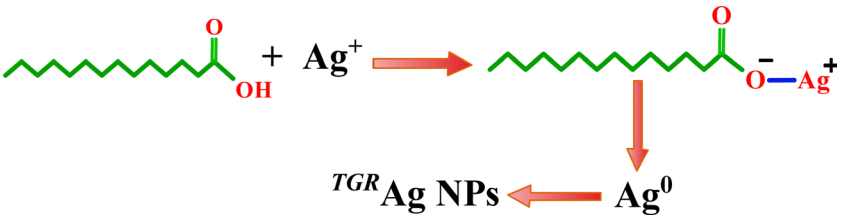

Fig. 2 Reaction mechanism of synthesis of ^{TGR}AgNPs.

by creating a protective phytochemical cage around the nanoparticles. Through this process, these phytochemicals prevent further aggregation through steric hindrance, resulting in the formation of a stable and uniformly shaped AgNPs.[54]

Interestingly, earlier studies on *Trillium govanianum* rhizome also indicated the presence of secondary metabolites such as fatty acid esters, glycosides, saponins, steroids, and carbohydrates in the rhizome.[55] In light of the above, these secondary metabolites might have mediated the reduction of silver, thereby leading to the synthesis of nanoparticles. As represented in Fig. 1, the obtained Ag^0 once formed nucleates into small clusters, which in turn create the nanoparticles. As observed in GC-MS analysis, the aqueous TGR extract is rich in diverse phytochemicals with an ability to effectively chelate metal ions and convert them into nanoparticles. The ability to produce NPs is ascribed to their abundance of essential functional groups, including numerous hydroxyl and carboxylic acid groups, as depicted in Fig. 1. As a result, the abundant phytochemicals, such as palmitic acid in the extract, facilitated the easy conversion of Ag^+ to Ag^0 through bioreduction (Fig. 2). Additionally, the organic functional groups present in the extract can bind to the surface of silver nanoparticles, preventing their aggregation and oxidation.

4.2. Characterization of ^{TGR}AgNPs

UV-vis spectroscopy. Generally, the electrons of a metal element surface oscillate on exposure of a nanoparticle to light of a specific wavelength, which in turn are responsible for strong absorption and scattering properties of the nanoparticle.[56] Owing to this, the green synthesis of ^{TGR}AgNPs was confirmed by UV-visible spectroscopy. As shown in Fig. 3a, the aqueous extract of *Trillium govanianum* rhizome did not show any specific absorption peak. However, after mixing the aqueous silver nitrate solution with aqueous extract of *Trillium govanianum* rhizome, distinct absorption maximum at 426 nm was observed due to surface plasmon resonance (SPR), which is the size-dependent property of the nanoparticles. Generally, the conduction electrons of the nanoparticle surface oscillate on exposure to light of a specific wavelength, which in turn are responsible for the strong absorption and scattering properties of the nanoparticle. The evolution of the surface plasmon absorption bands observed during the synthesis of NPs from 15 minutes to 3 hours are shown in Fig. 3(a). As shown in Fig. 3(a), the intensity of the observed SPR band at 426 nm increased with reaction time. It is reported that the spherical NPs result in a single SPR band, while anisotropic particles

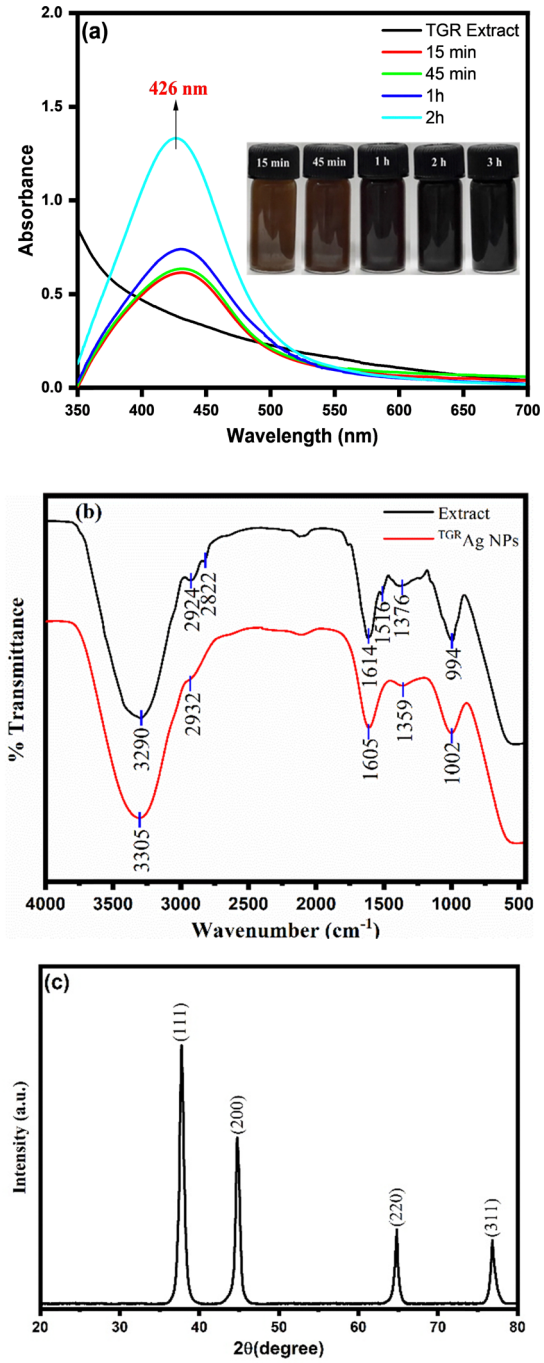

Fig. 3 (a) UV-visible spectra of TGR extract and TGR extract synthesised AgNPs (Inset: optical images of ^{TGR}AgNPs at different time intervals), (b) FTIR spectra and (c) XRD diffractogram of ^{TGR}AgNPs.

exhibit 2 or more bands depending on the particle size and shape. In our case, observation of a single sharp SPR band indicates the formation of spherical-shaped nanoparticles with homogenous distribution. Moreover, the synthesis of NPs within 15 minutes indicates that the TGR extract speeds up the biosynthesis of the nanoparticles, probably due to the efficient reducing capability of phytochemicals present in the plant extract.

In addition, the stability of the ^{TGR}AgNPs was monitored at different temperatures, and the ageing effect was studied for 5 days (Fig. S2a and b, ESI†). As can be seen from the results, ^{TGR}AgNPs showed a characteristic SPR λ_{max} peak at 426 nm with a slight increase in absorption intensity without any shift in the peak wavelength over the time period of 5 days (Fig. S2a, ESI†). In fact, the obtained suspension maintained a high degree of stability even after extended periods of storage and ageing. The existence of AgNPs during the first stages of the reaction indicated that even a short reaction time is sufficient for the formation of the nanoparticles. Furthermore, the thermal stability of the synthesized ^{TGR}AgNPs was monitored by heating the reaction mixture at different temperatures *i.e.*, 5, 30, 40, and 60 °C (Fig. S1b, ESI†). At 60 °C, the maximum intensity of SPR λ_{max} peak was still observed at 426 nm with a temperature-dependent increase in absorption, which in turn demonstrates the temperature-induced increased rate of AgNP synthesis. Overall, the results concluded that while increasing the reaction temperature, the absorbance intensity also increased without any shift in the peak position.

4.3. FTIR analysis

Identification of the secondary metabolites, most probably responsible for the reduction and capping of ^{TGR}AgNPs, was accomplished by using FTIR spectroscopy. The FTIR spectra of the TGR extract exhibited prominent absorption peaks at 3290, 2924, 2822, 1614, 1516, 1376, and 994 cm^{-1}, as depicted in Fig. 3b. The phytochemical examination of the TGR extract indicated the presence of flavonoids, alkaloids, steroids, rosins, saponins, and proteins. The FTIR spectrum of ^{TGR}AgNPs exhibited prominent absorption peaks at 3305, 2932, 1605, 1359, and 1002 cm^{-1}, indicating the presence of phytoconstituents that function as capping agents (Fig. 3b). Comparative analysis of the FTIR peaks of the ^{TGR}AgNPs and TGR extract identified a complete absence of the peak 1516 cm^{-1} in the nanoparticles, implying that the fatty acids with –C═O functional groups are responsible for the stabilization and fabrication of nanoparticles. Furthermore, significant changes in other peak positions were observed in the FTIR spectra of the TGR extract, corresponding to ^{TGR}AgNPs, which can be attributed to the reduction, capping, and stabilization of the synthesized ^{TGR}AgNPs. The signal at 3290 cm^{-1} shifted to 3305 cm^{-1}, indicating the participation of phenolic compounds in the TGR extract in stretching O–H bonds. The peak observed at 2932 cm^{-1} is a result of the stretching of the C–H bonds in the methylene or aliphatic group and is also a distinctive feature of triterpenoid saponins. The band observed at 1614 cm^{-1} shifted to a higher wavenumber of 1605 cm^{-1}, indicating the presence of alkenyl or aromatic stretching. The band observed at 1359 cm^{-1} indicates the existence of the –C–O stretching, characteristic of phenol or tertiary alcohols. Similarly, the band at 1002 cm^{-1} corresponds to the O–H stretching of the phenol group. Most of the peaks correspond to the phenolic groups of the polyphenols, triterpenoids, alkaloids, steroids, and tannins adequately present in the extract. They might be, in turn, responsible for the formation of ^{TGR}AgNPs. Similar to our results, earlier studies of FTIR characterization of AgNPs have indicated that the peak at 3340 cm^{-1} is due to O–H bonds in OH functional groups, C–H stretching of alkanes resulted in peaks at 2925 cm^{-1}, peak at 1736 cm^{-1} corresponds to carbonyl groups and a distinct peak at 1636 cm^{-1} may be related to C═O stretching.[57,58] On the other hand, an obvious peak at 1376 cm^{-1} could be related to the stretching vibrations of alcohols, ethers, esters, carboxylic acids, and amino groups, while the peak at 994 cm^{-1} might be attributed to C–H bending vibrations.[57] In addition to this, it has been shown that the FTIR spectrum of green synthesized AgNPs exhibited absorption peaks at 3305 cm^{-1}, 2932 cm^{-1}, 1605 cm^{-1}, 1359 cm^{-1} and 1002 cm^{-1} corresponding to O–H, C–H, alkene (C═C), bending (C–H) and C–O bonds, respectively.[58] Altogether, FTIR findings for the ^{TGR}AgNPs are quite consistent with the phytochemical analysis of the TGR extract.

4.4. XRD analysis of ^{TGR}AgNPs

The biosynthesized ^{TGR}AgNPs were analysed by XRD for their crystalline nature and phase purity, as shown in Fig. 3c. The XRD pattern of ^{TGR}AgNPs exhibited four prominent diffraction peaks at 2θ = 37.79, 44.77, 64.89, and 76.70° indexed as (111), (200), (220), and (311) (JCPDS file No. 04-0783).[59] The high intense peak in the XRD spectrum demonstrates the polycrystalline phase composition of ^{TGR}AgNPs, confirming the production of face-centered cubic (fcc) crystalline ^{TGR}AgNPs. The diffraction peaks of (111), (200), (220), and (311) planes were also observed in the green synthesis of AgNPs.[60] XRD patterns confirmed the structure of ^{TGR}AgNPs as a cubic structure and confirmed the purity of the as-prepared AgNPs using TGR extract. Moreover, several reducing agents in the TGR extract are responsible for stabilizing ^{TGR}AgNPs, thus providing them with a crystalline structure quite well studied in various biosynthesized nanoparticles. The average crystallite size of ^{TGR}AgNPs was calculated using the Debye–Scherrer formula[61] using eqn (5). From this, the calculated average crystallite size of the ^{TGR}AgNPs was found to be ~32 nm. Overall, the results demonstrated that ^{TGR}AgNPs exist as small and monodispersed nanoparticles.

$$D = \frac{k\lambda}{\beta \cos\theta} \quad (5)$$

where the average size of the nanoparticles is represented by D, the geometric factor is denoted by k (0.9), λ refers to the wavelength of the X-ray radiation source, and β represents the angular FWHM (full width at half maximum) of the XRD peak at the diffraction angle θ.

4.5. Particle size analysis

The dynamic light scattering measurements were performed to determine the hydrodynamic diameter, particle size distribution (PSD), and polydispersity index (PDI) of ^{TGR}AgNPs. The particle size distribution and zeta potential of the ^{TGR}AgNPs is shown in Fig. S3(a and b) (ESI†). The average hydrodynamic size of ^{TGR}AgNPs was 131.9 nm, which is larger than the size observed in the TEM analysis. The phytochemicals present in the TGR act as capping agents, resulting in the increase of the hydrodynamic diameter of ^{TGR}AgNPs. The PDI value of ^{TGR}AgNPs was found to be 0.148, indicating that they were relatively polydispersed.

Zeta potential, regarded as an indicator of surface charge potential, is an important parameter for understanding the stability of nanoparticles in aqueous suspensions. Any charge on the surface of nanoparticles provides stability and prevents aggregation of nanoparticles by repulsion between like-charged particles. In view of this, the Zeta potential value of ^{TGR}AgNPs was found to be −38.0 mV (Fig. S3(b), ESI†). A high absolute value of zeta potential specifies a high electrical charge on the surface of the nanoparticles, which in turn might lead to strong repellent forces among the particles, thus preventing their agglomeration.[62] Moreover, the strong negative charge of ^{TGR}AgNPs demonstrates negative charges all across the nanoparticles surface, indicating their great colloidal dispersivity and long-term stability. Literature studies have reported that nanoparticles with a zeta potential value higher than +30 mV or lower than −30 mV are considered quite stable in the dispersion medium.[63] Results obtained here indicate the successful formation of the nanoparticles with long-term stability. The negative potential value might be due to the absorption of capping biomolecules present in the TGR extract. Overall, the results are quite consistent with some earlier reports, such as *F. religiosa* leaf extract mediated synthesis of AgNPs.[64]

4.6. Morphological analysis

Scanning electron microscopy (SEM) analysis was used to determine the surface morphology of ^{TGR}AgNPs, and energy dispersive X-ray analysis (EDX) was used to investigate the elemental composition of the as-prepared ^{TGR}AgNPs. The nanoparticles were primarily observed to be uniformly dispersed in polymorphic forms, with a small percentage being slightly aggregated, ellipsoidal, and irregularly granulated (Fig. 4a and b). Similar kinds of nanoparticles were observed during the *Taraxacum officinale* mediated synthesis of AgNPs.[65] The size of ^{TGR}AgNPs from SEM micrographs was found to be 30–50 nm. From the EDX spectrum of ^{TGR}AgNPs shown in Fig. 4c, a high-intensity peak of Ag metal at 3 keV indicates that silver is the major constituent (80.30%) in the prepared sample. Other constituents like carbon (16.70%) and oxygen (3%) could be due to the presence of phytochemical compounds of TGR extract on the surface of the ^{TGR}AgNPs, validating phytochemicals as the capping and reducing agents.

Furthermore, the surface morphology, size and particle size distribution were confirmed from TEM analysis of the ^{TGR}AgNPs at different nanoscale magnifications (Fig. 5a and b). The TEM images at different nanoscale magnifications revealed that ^{TGR}AgNPs are slightly agglomerated and nearly spherical to irregular shape. The particle size distribution histogram, (Fig. 5c), obtained using ImageJ software, represents the size distribution of the particles which in turn confirms the polydispersity of ^{TGR}AgNPs. Moreover, the results revealed that the determined particle size varied between 15–55 nm (Fig. 5c). The average particle size of ^{TGR}AgNPs was found to be ∼38 nm, nearly similar to the crystallite size and SEM observation of these nanoparticles. As can be seen in Fig. 5e, the high-resolution TEM images showed characteristics of lattice fringes with a lattice fringe width of 0.242 nm, corresponding to Ag (111) crystal planes.[66] In addition, a typical selected-area diffraction (SAED) pattern demonstrates the continuous ring patterns without additional diffraction spots and rings of secondary phases, revealing their crystalline structure. ^{TGR}AgNPs exhibit four bright rings, indexed as (111), (200), (220), and (311) lattice planes of the crystalline silver face-centered cubic (fcc) structure, respectively (Fig. 5f).[67] In addition to this, the results observed in the SAED pattern (Fig. 5f) are in good agreement with the XRD results of ^{TGR}AgNPs, wherein the most intense peak observed at 37.79° 2θ is related to Ag (111) crystal planes.[68]

4.7. Antioxidant activity

Based on our GC-MS analysis and earlier studies, TGR contains a range of phytochemicals, including fatty acids, steroids, carbohydrates, alkaloids, phenols, *etc.* Moreover, several authors have also reported the antioxidant activity of the rhizome of *Trillium govanianum*.[69] In light of this, during the

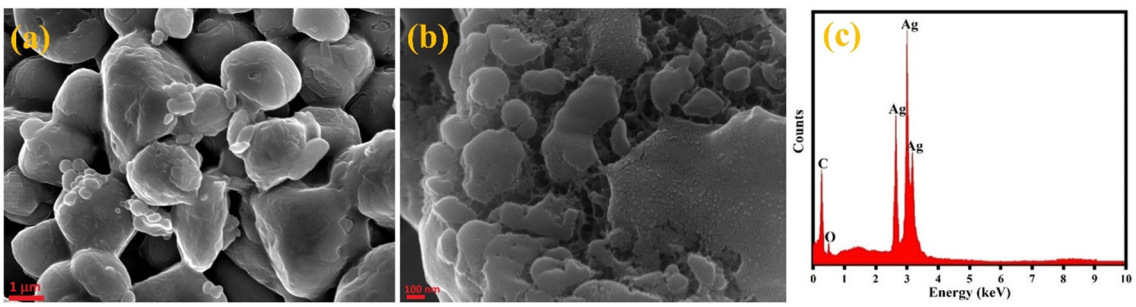

Fig. 4 SEM micrographs at (a) 1 µm (b) 100 nm and (c) EDX spectrum of ^{TGR}AgNPs.

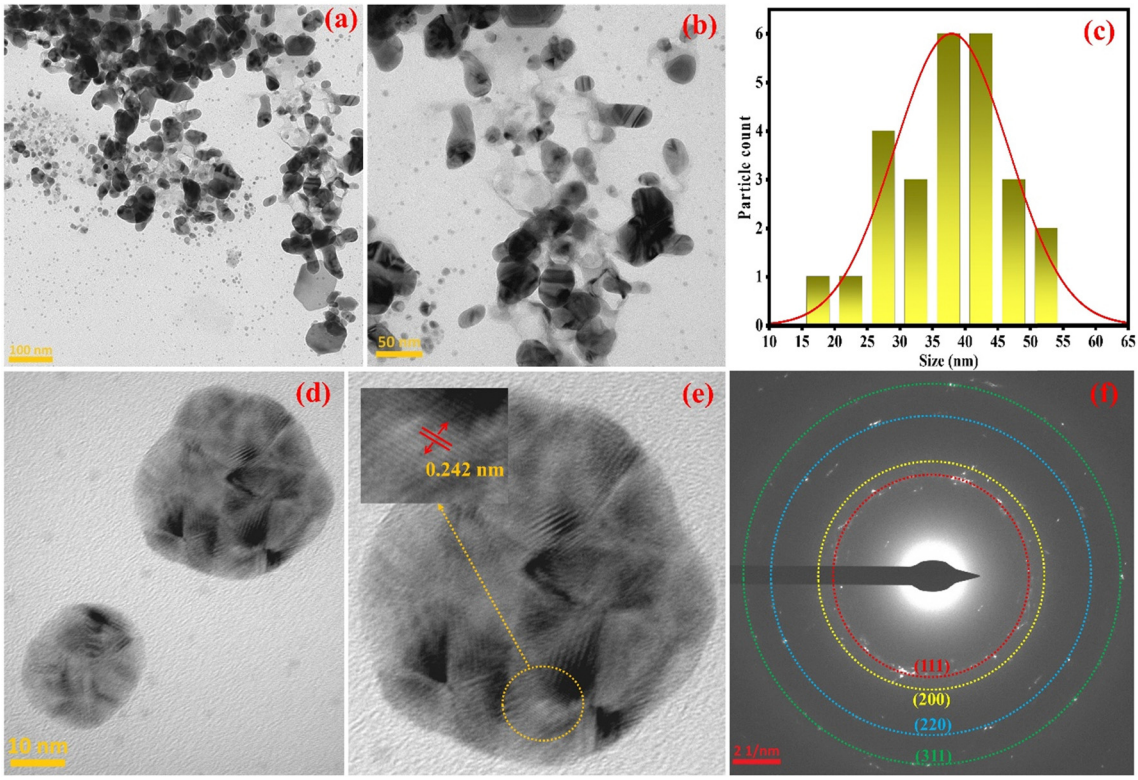

Fig. 5 TEM micrographs at (a) 100 nm (b) 50 nm nanoscale magnifications, (c) size distribution histogram, (d) HR-TEM (e) HR-TEM with zoom-in showing lattice fringes and (f) SAED patterns of ^{TGR}AgNPs.

green synthesis of nanoparticles by ^{TGR}AgNPs, it is quite expected that the synthesized ^{TGR}AgNPs might be coated with the bioactive constituents of the extract. Previous literature reports have also shown possible capping of bioactive constituents during the green synthesis of nanoparticles.[70] To evaluate this, DPPH assay was performed where DPPH is regarded as a lipophilic radical whose colour changes from purple to yellow on accepting hydrogen and electrons from the donor.[71] In this, different concentrations of ^{TGR}AgNPs (0.05–0.25 mg mL^{-1}) and TGR extract (0.05–0.25 mg mL^{-1}), used as a control, were titrated into DPPH solution for the purpose of free radical scavenging. Ascorbic acid (0.3–8.3 μg mL^{-1}) was used as a standard. The standard showed the radical scavenging activity of 81.5% at a concentration of 8.3 μg mL^{-1}. As shown in Fig. 6a, ^{TGR}AgNPs revealed a significant dose-dependent free radical scavenging activity with the highest scavenging of 85.7% ± 1.4% at 0.25 mg mL^{-1} and the lowest of 29.8 ± 1.25% at 0.05 mg mL^{-1}. On the other hand, the highest and lowest scavenging activities of TGR extract were, respectively, found to be 65.2 ± 0.7% and 19.5 ± 1% at 0.25 mg mL^{-1} and 0.05 mg mL^{-1}. Similar studies with green synthesized silver nanoparticles also exhibited potential radical scavenging activity with concentration dependent inhibition.[72] Moreover, the observed free radical scavenging activities of ^{TGR}AgNPs were quite comparable to the already reported green synthesized silver nanoparticles.[73] It has been shown that scavenging ability of *Chenopodium murale* leaf extract-mediated silver nanoparticles was dose dependent with a highest and lowest activities of 65% and 13%, respectively.[74] Similarly, *A. tribuloides* root extract-mediated AgNPs exhibited 64% activity while aqueous extract of *E. scaber* mediated showed 85% activity.[75,76] In comparison to these studies, the ^{TGR}AgNPS exhibited much significant antioxidant activity and thus can serve as a potent antioxidant agent with a highest scavenging activity of ~86%. Interestingly, a number of studies have shown that green synthesized nanoparticles show better radical scavenging potential as compared to chemically synthesized ones,[77,78] probably due to the presence of a bioactive capping agents on their surfaces. Overall, results infer that ^{TGR}AgNPs exhibited potential antioxidant activity possibly due to the presence of the coated phytochemicals, which might include palmitic acid, diosgenin, astaxanthin and alpha tocopherol, observed during the GC MS analysis of the TGR extract (Table S1, ESI†).

4.8. Hemo-compatibility of ^{TGR}AgNPs

With the increased clinical application of AgNPs, their biosafety is vital. Hence, assessment of hemo-compatibility of the synthesized ^{TGR}AgNPs is necessary in light of blood-contacting medical appliances. Generally, characteristics of AgNPs, such as size and surface area, interfere with their hemolytic activity. Normally, hemolysis of RBCs is due to their compromised membranes, resulting in hemolytic leakage. ^{TGR}AgNPs were elucidated for hemocompatibility by monitoring cytotoxicity on RBCs through haemoglobin (Hb) release. For that,

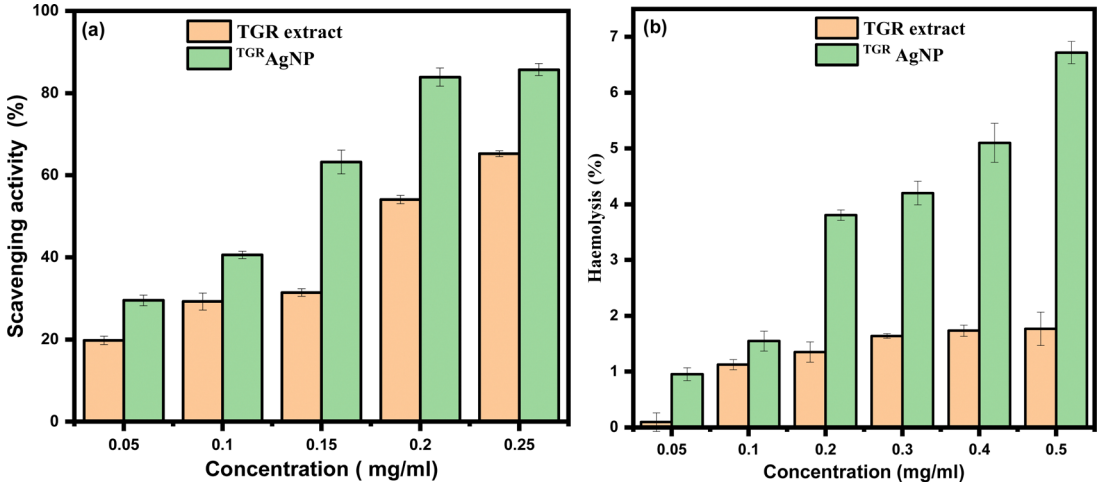

Fig. 6 Antioxidant and hemolytic activity of ^{TGR}AgNPs: Panels represent (a) plot of percentage scavenging activity against different concentrations of ^{TGR}AgNPs with a statistical difference of $p < 0.001$ (mean ± SD, $n = 3$) and (b) plot of percentage hemolysis of RBCs against different concentrations of ^{TGR}AgNPs with $p \leq 0.05$ (mean ± SD, $n = 3$).

suspended RBCs were titrated with different concentrations (0.05, 0.1, 0.2, 0.3, 0.4 and 0.5 mg mL^{-1}) of ^{TGR}AgNPs. Results indicated a maximum hemolysis of 6 ± 0.2% at the highest concentration (0.5 mg mL^{-1}) of ^{TGR}AgNPs with a minimum of 0.95 ± 0.1% at its lowest concentration (0.05 mg mL^{-1}). TGR extract was used as a control, wherein the extract exhibited the highest haemolysis of 1.76 ± 0.3% at 0.5 mg mL^{-1} with a hemolysis of 0.09 ± 0.006% at its lowest concentration. PBS buffer (negative control) and TritonX-100 (positive control) exhibited 0.05% and 95% hemolysis, respectively. As shown in Fig. 6b, a hemolytic activity of 6.1% was observed in 0.5 mg mL^{-1}, which is slightly higher than the acceptable value (*i.e.* 5%) for the clinical applications of the nanoparticles as per World Health Organization (WHO) guidelines. Except this, all other concentrations of the ^{TGR}AgNPs are well below the recommended value of WHO. Overall, the results infer that the synthesized ^{TGR}AgNPs are largely compatible with no significant hemolytic effect on RBCs. A number of studies have also observed the biocompatibility of green synthesized nanoparticles, such as *cannabis sativa* root extract mediated silver nanoparticles exhibited ∼7% haemolysis, and AgNPs synthesized from *Annona reticulata* leaves extract showed ∼14% haemolysis.[79,80] Moreover, a number of polymeric nanoparticles have been shown to exhibit >10% hemolysis. Interestingly, as compared to these reports, the ^{TGR}AgNPs exhibit significant biocompatibility with promising biomedical applications. More importantly, green-synthesized nanoparticles are generally more biocompatible than chemically synthesized nanoparticles.[81] So far, the actual mechanism for AgNPs-induced hemolysis is still not clear. However, it has been shown that on coming in contact with the body fluids, metallic silver undergoes ionization, leading to the release of Ag^+, as per the response of the nanoparticle surface area, which in turn induces hemolysis of cells like RBCs, at least under *in vitro* conditions.[82] In biological systems, neutralizing the ionized silver ions by ions like chloride, sulfide, *etc.*, makes them unavailable for hemolytic activity. Moreover, the interaction of nanoparticles with other cellular components, such as proteins and antioxidants, might result in their cell lysis activity. In fact, literature studies report that there is always a release of Ag^+ ions on the interaction of AgNPs with the RBC membrane.[83]

4.8. Cytotoxicity activity

The biological role of AgNPs has gained great interest in diagnosing and bioremediation of cancers. In this study, preliminary screening of the biosynthesized ^{TGR}AgNPs for cytotoxicity against the HCT-116 cell line was carried out through MTT Assay. 5-Fluorouracil (5FU), used as a standard, exhibited a cytotoxicity of 92.8 ± 2.8% at 4 μg mL^{-1}. As shown in Fig. 7a, a concentration-dependent increase in cytotoxicity was observed with 84.4 ± 4.1% at 0.5mg mL^{-1} of ^{TGR}AgNPs. An IC_{50} value of 0.17 mg mL^{-1} was observed for ^{TGR}AgNPs-induced cytotoxicity. TGR Extract was used as a control. The highest cytotoxicity for extract was found to be 78 ± 4.4% at 0.5 mg mL^{-1}. A number of other studies have also shown cytotoxicity of green synthesized nanoparticles. *C.nudiflora* mediated silver nanoparticles showed potent cytotoxicity against HCT-116 colon cancer cells with an IC_{50} value of 100 μg mL^{-1}.[84] *S. Jambolanum* AgNPs caused a significant decrease in cell viability of the MCF-7 cells when compared to the plant extract.[85] The AgNPs synthesized using *Chaetomorpha linum* exhibited dose-dependent toxicity, while *Putranjiva roxburghii* seed extract-mediated AgNPs showed anti-cancerous activity against HCT-116 cell lines at a concentration of 10 mg mL^{-1}.[86,87] Another study reported *Avicennia marina* synthesized-AgNPs exhibited anticancer activity at 80 μg mL^{-1}.[88] Moreover, it is a well-established fact that as compared to chemically synthesized nanoparticles, green synthesized nanoparticles are usually found to be more cytotoxic.[89,90] Overall, a number of studies have reported the cytotoxicity activity of green synthesized silver nanoparticles,[91] wherein numerous effects have been combined to elucidate the

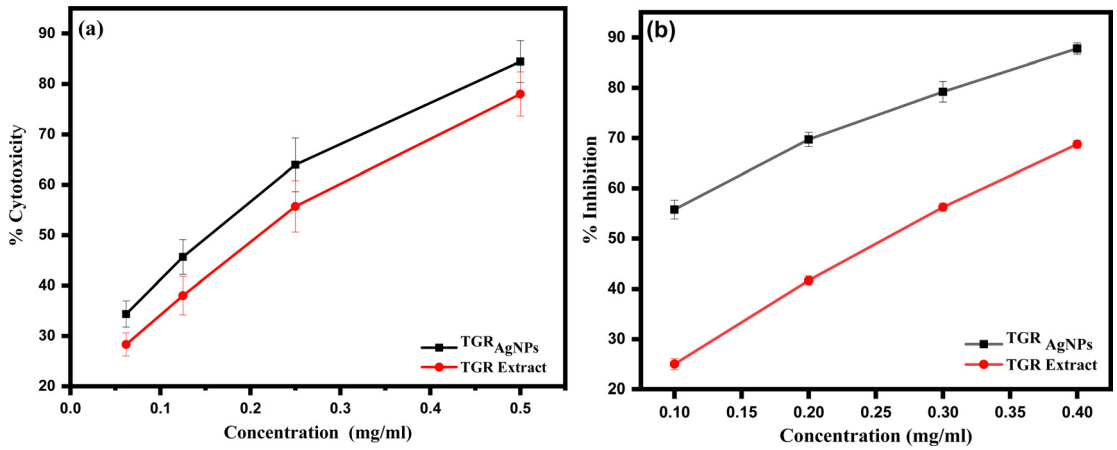

Fig. 7 Cytotoxicity and anti-inflammatory activities of AgNps: Panels represent – (a) cell viability assay of HCT-116 cell line as plot of percentage cytotoxicity against different concentrations of ^{TGR}AgNPs and the TGR extract, $p < 0.05$, and (b) anti-inflammatory activity of ^{TGR}AgNPs as a plot of percent protein denaturation inhibition against different concentrations of ^{TGR}AgNPs and the TGR extract as control, $p \leq 0.05$.

mechanism of NP-induced cytotoxicity. Among others, one of the plausible mechanisms is the ability of nanoparticles to scavenge free radicals.[92] Observed antioxidant activity of ^{TGR}AgNPs, in the present study also supports the free radical-induced cytotoxicity of the nanoparticles. Interestingly, hexadecenoic acid (palmitic acid) has been shown to exhibit potent anticancer activity.[93] Palmitic acid (PA) has demonstrated efficacy in inhibiting the proliferation of tumor cells, promoting tumor cell apoptosis, and influencing the cell cycle in most of the cancers including gastric, cervical, liver, breast, colorectal and other types of tumors. It has been shown that palmitic acid influences signal transduction pathways related to membranes, leading to tumor cell proliferation inhibition, induction of apoptosis, suppression of cell invasion and migration, and increase in the efficacy of chemoradiotherapy drugs. Additionally, PA is shown to possess immune system regulating properties and induces cellular autophagy, further contributing towards its anti-cancer mechanisms.[94] Interestingly, the same compound has been observed as the most abundant phytochemical in the GC-MS analysis of the TGR extract and thus might be present as a capping agent on the AgNPs (Table S1, ESI†).

4.9. Anti-inflammatory activity

Protein denaturation is regarded as a primary cause of inflammation, wherein denaturation is shown to produce auto antigens in diseases like arthritis, diabetes, and cancer, which are causes of inflammation.[95] Hence, inhibition of protein denaturation should prevent inflammation. In light of this, the green synthesized ^{TGR}AgNPs were evaluated for their ability to inhibit the denaturation of BSA, a model protein for such assays. Sodium diclofenac was used as a standard drug and acted as a positive control. As shown in Fig. 7b, a dose-dependent anti-inflammatory potential of ^{TGR}AgNPs was observed with the highest inhibition of 87.7 ± 1.1% at 0.4 mg mL^{-1} of NPs. On the other hand, TGR extract showed the maximum inhibition of 68.75 ± 0.8% at 0.4 mg mL^{-1}. In contrast, the positive control showed a maximum level of 93% at 0.4 mg mL^{-1}. Overall, the results infer that ^{TGR}AgNPs exhibits more potent anti-inflammatory activity as compared to the extract indicating the enhanced accessibility and activity of the nanoparticles. Similar studies with *A. tribuloides* root extract showed inhibition of 69% at the highest concentration of 500 μg mL^{-1}.[96] *A. lycoctonum* mediated Ag NPs showed an anti-inflammatory effect in a dose-dependent manner with inhibition of 91.78% at the highest concentration (500 μg mL^{-1}).[97] Another study reported silver nanoparticles from *Microsorum punctatum* were effective in inhibiting thermally induced albumin denaturation at different concentrations with a highest inhibition of 69% at 100 μg mL^{-1}.[98] The anti-inflammatory activities of synthesized Ag nanoparticles from *Justica wynaadensis*, showed an inhibition of around 40% at 200 μg mL^{-1}.[99] Silver nanoparticles synthesized from leaf extract of *Madhuca longifolia* have been shown to exhibit protein denaturation inhibition of 53.15 ± 0.87% at a concentration of 500 μg mL^{-1}.[100] As compared to these reports, ^{TGR}AgNPs showed a significant inhibition of 87.7% at 0.4 mg mL^{-1} of NPs. In light of the above results, the possible coating of the biosynthesized nanoparticles by the secondary metabolites like palmitic acid, diosgenin, astaxanthin, *etc.*, identified in GC/MS analysis, might be responsible for the anti-inflammatory effects of nanoparticles. Moreover, TGR extract, as such, has been reported to exhibit anti-inflammatory activity.[101] Some of the earlier studies also suggest that the lysosomal components released by neutrophils at the site of inflammation might be suppressed by the coated secondary metabolites of the nanoparticles.[102]

4.10. DNA damage protection assay

The green synthesized ^{TGR}AgNPs were evaluated for their potential to protect against Fenton-induced calf thymus DNA damage. As can be seen in Fig. 8A, the untreated (control) calf thymus DNA (lane 1) and ^{TGR}AgNPs treated DNA maintained their integrity. However, the Fenton reagent induced damage to

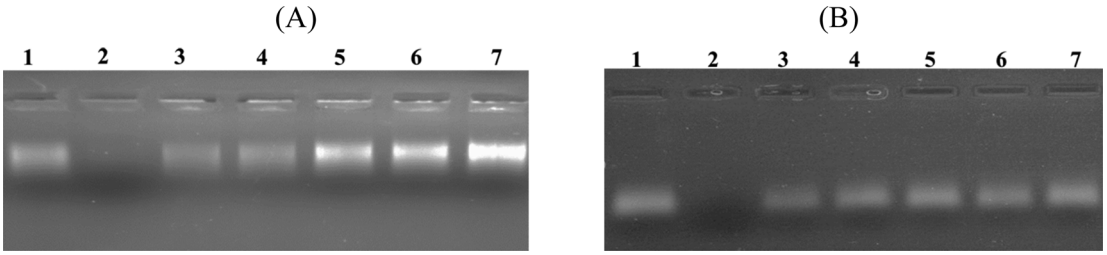

Fig. 8 Representative Agarose gel electrophoretic pattern of calf thymus DNA damage in the presence and absence of ^{TGR}AgNPs (A) and TGR extract (B). Different lanes in Panel (A) represent – Lane 1: untreated DNA, lane 2: damaged DNA exposed to Fenton's reagent, lanes 3–6: DNA damage in the presence of 0.1 mg mL^{-1}, 0.3 mg mL^{-1} and 0.9 mg mL^{-1} of ^{TGR}AgNPs, respectively and lane 7: DNA damage in presence of catechin. Different lanes in Panel (B) represent – Lane 1: untreated DNA, lane 2: damaged DNA exposed to Fenton's reagent, lanes 3–6: DNA damage in the presence of 0.1 mg mL^{-1}, 0.3 mg mL^{-1} and 0.9 mg mL^{-1} of TGR Extract, respectively and lane 7: DNA damage in presence of catechin.

the DNA is observed as the complete absence of the DNA band in the electrophoresis gel (lane 2). As seen in lanes 3–6 (Fig. 8A), ^{TGR}AgNPs were able to protect the Fenton-induced DNA damage, as evidenced by the appearance of intact DNA bands in the lanes. A concentration-dependent protection was observed as reflected by the increased intensity of the bands with increased concentration of ^{TGR}AgNPs. Catechin was used as standard (lane 7). Moreover, a concentration-dependent protective effect of the extract was observed. However, it was not as pronounced as that of the nanoparticles, as indicated by the intensity and intactness of the protein bands (lanes 3–6, Fig. 8B. Overall, the results infer that synthesized ^{TGR}AgNPs are able to protect the DNA from free radical induced damage possibly due to their hydroxyl radical scavenging potential as observed in Fig. 8. Similar results have been reported for *Rhus coriaria L.* mediated silver with a concentration dependent DNA damage protective effect.[103]

In summary, ^{TGR}AgNPs demonstrated comparatively higher bioactivity for the tested activity assays when compared to the reported green-synthesized silver nanoparticles. For this, a comparative analysis of the activities exhibited by ^{TGR}AgNPs with the reported green-synthesized nanoparticles is summarized in Table S2 (ESI†).[104–117] As can be inferred from Table S2 (ESI†), the observed antioxidant activity of ^{TGR}AgNPs stands out, exhibiting a maximum scavenging of 85.7%, which is notably higher than most of the other green-synthesized silver nanoparticles. For example, nanoparticles from *N. leucophylla*-mediated nanoparticles displayed 79% activity, while *A. tribuloides* and *E. scaber*-mediated nanoparticles showed 64% and 85%, respectively.[75,76] With respect to hemocompatibility, the ^{TGR}AgNPs exhibited a hemolysis of 6.1% at 0.5 mg mL^{-1}, which is much better than that of *Cannabis sativa* root extract-mediated AgNPs, with a hemolysis of 7% at 0.2 mg mL^{-1}, and polymeric nanoparticles (>10%).[79] For cytotoxicity,

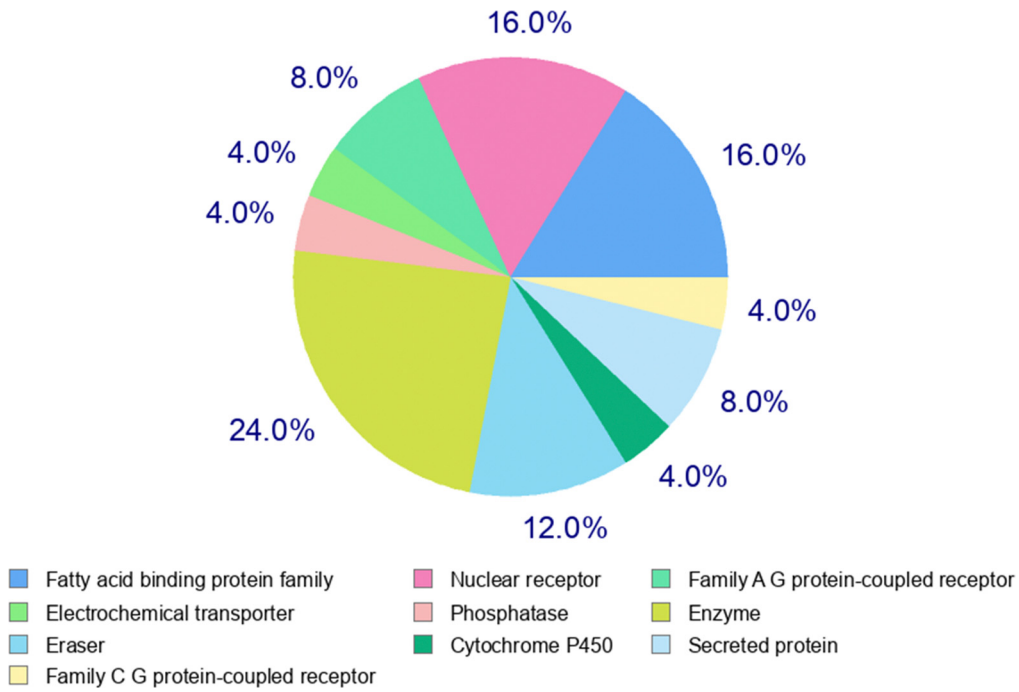

Fig. 9 Pie-chart representing the possible top ten target proteins of palmitic acid.

^{TGR}AgNPs induced 84.4% cytotoxicity at 0.5 mg mL^{-1} (IC_{50} value of 0.17 mg mL^{-1}), which is quite comparable to that of *C. nudiflora*-mediated AgNPs (IC_{50} = 0.1 mg mL^{-1}) and much better than that of *Putranjiva roxburghii* AgNPs (IC_{50} = 0.5 mg mL^{-1}).[84,87] Moreover, the anti-inflammatory potential of ^{TGR}AgNPs (87.7% inhibition) exceeds the *A. tribuloides* root extract (69%) and *Madhuca longifolia* -mediated AgNPs (53.15% at 500 μg mL^{-1}).[96,100] Lastly, ^{TGR}AgNPs provided effective protection against Fenton-induced DNA damage, comparatively at lower concentration range as compared to *Rhus coriaria* AgNPs, showing a potent concentration-dependent protective effect.[103] In summary, ^{TGR}AgNPs exhibit reasonably higher bioactivity across all the tested assays, as compared to the reported results, underlining their potential as a potent bioactive material in future therapeutic applications, particularly in the areas of antioxidant therapy, cancer and inflammation control.

5. Network pharmacology based *in silico* analysis

As per GC MS analysis, hexadecenoic acid (palmitic acid) is the most prominent secondary metabolite in the TGR extract (Table S1, ESI†). In order to elucidate the possible reasons for the observed activity of the AgNPs, *in silico* network pharmacology analysis of palmitic acid was carried out. Palmitic acid ($C_{16}H_{32}O_2$) is a saturated fatty acid with a molecular weight of 256.42. It has 18 heavy atoms and no aromatic heavy atoms. The fraction of sp^3 carbons is 0.94, indicating that the molecule is mostly composed of saturated carbon atoms. Palmitic acid has 14 rotatable bonds, 2 hydrogen bond acceptors, and 1 hydrogen bond donor. In terms of physicochemical properties, palmitic acid has a mean molecular refractivity (MR) of 80.80, a topological polar surface area (TPSA) of 37.30, and various logP values (iLOGP, XLOGP3, WLOGP, MLOGP, Silicos-IT Log *P*,

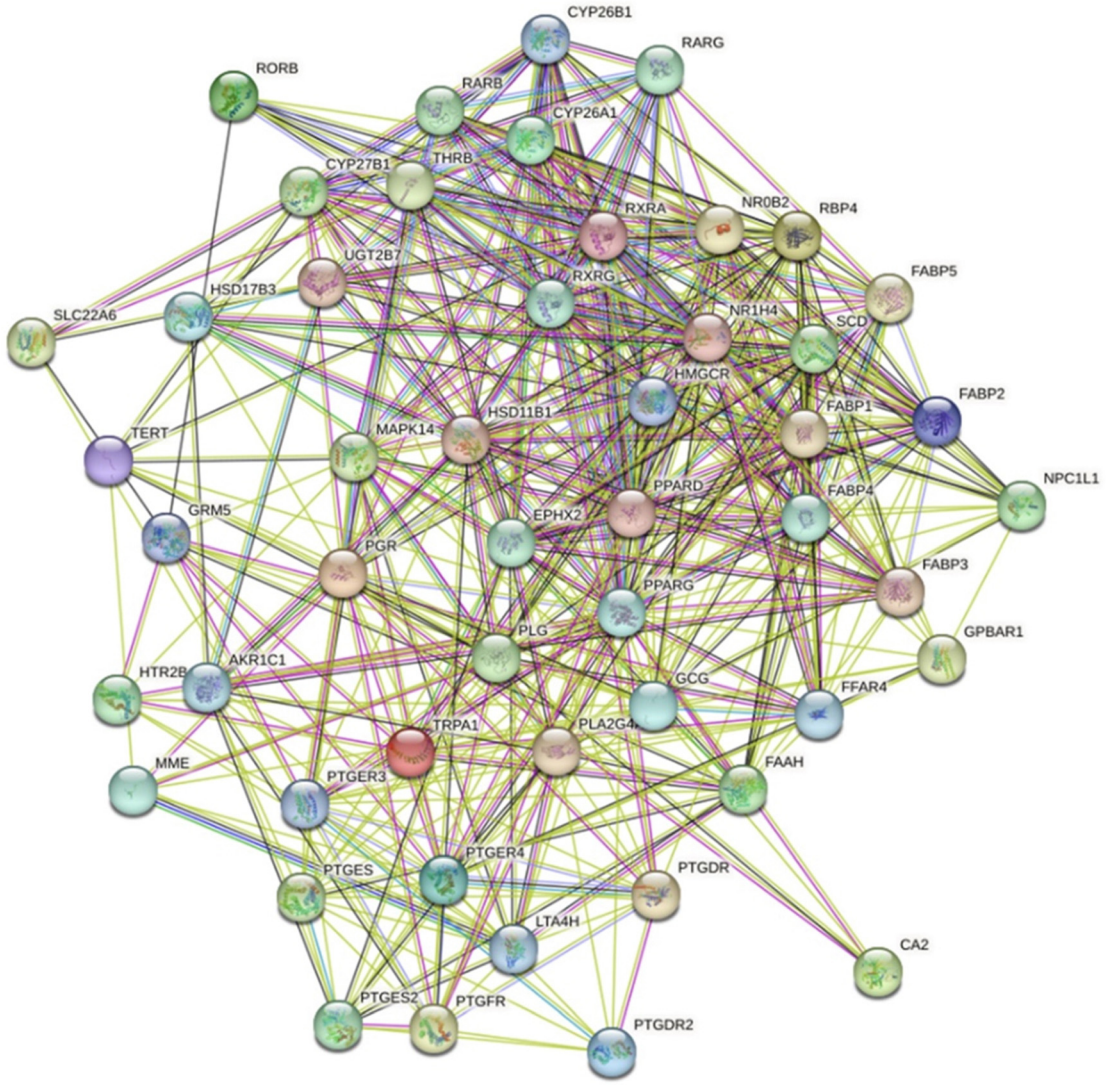

Fig. 10 The PPI interaction network of the common target genes of palmitic acid. Target genes are depicted as nodes while as the relationships between them are expressed as edges.

Consensus Log *P*). These values provide insights into the molecule's lipophilicity and potential for permeation across biological membranes. The compound was analysed for its physicochemical characteristics and pharmacokinetic parameters, including ADME analysis. The ADME profile of palmitic acid indicates that it is moderately soluble, with an ESOL Log *S* value of −5.02. It has a relatively low solubility in both the ESOL and Ali prediction models. Palmitic acid is found to exhibit good gastrointestinal absorption and is also quite likely to cross the blood–brain barrier system.[118] Moreover, it is not a P-glycoprotein substrate and does not inhibit CYP enzymes.[119] Overall, based on the provided data, palmitic acid shows favourable ADMET properties in terms of solubility, absorption, and permeability, which makes it a potentially bioavailable compound with lower toxicity issues.

For the identification of palmitic acid-related drug targets, Web-based servers PharmMapper and Swiss Target were used for identification of possible target proteins for palmitic acid. Among the identified target proteins, the top 10 targets are shown in Fig. 9. As can be seen in the figure, nuclear receptors, fatty acid binding proteins and commonly found cytosolic enzymes are the key targets followed by G-protein coupled receptors (family AG/CG protein coupled receptor) and cytochrome P450. Overall, the results indicate the palmitic acid is able to target some key proteins of the cellular system. Moreover, to delve deep into the mechanistic insights, protein–protein interaction (PPI) network and functional gene annotation analysis was also carried out. As can be seen in the Fig. 10, PPI network analysis identified 50 proteins with a total of 439 interactions. The observed number of interactions is significantly higher than the expected number of interactions (95) with a *p*-value of 0.005. Results suggest that the network is densely connected with a high degree of interactivity among the proteins.

Functional analysis of palmitic acid targets was also conducted using gene ontology (GO) and pathway analysis through Shiny GO. Enrichment analysis utilized data from various annotations and ontology resources. The analysis classified GO terms and pathways, based on biological functions, into three stages: biological process (BP), molecular function (MF), and cellular component (CC) (Fig. 11). Pathway-related data was extracted from the KEGG database. As the identified pathways associated with palmitic acid encompass a diverse array of biological processes and signalling cascades. These findings suggest the multifaceted roles of palmitic acid in cellular metabolism, signalling pathways, and hormonal signalling. KEGG pathway enrichment analysis of the aforementioned common target genes is shown in Fig. 12. Post exclusion of broad pathways, the top 20 signalling pathways are listed in Table 1. Specifically, the enrichment of pathways such as the

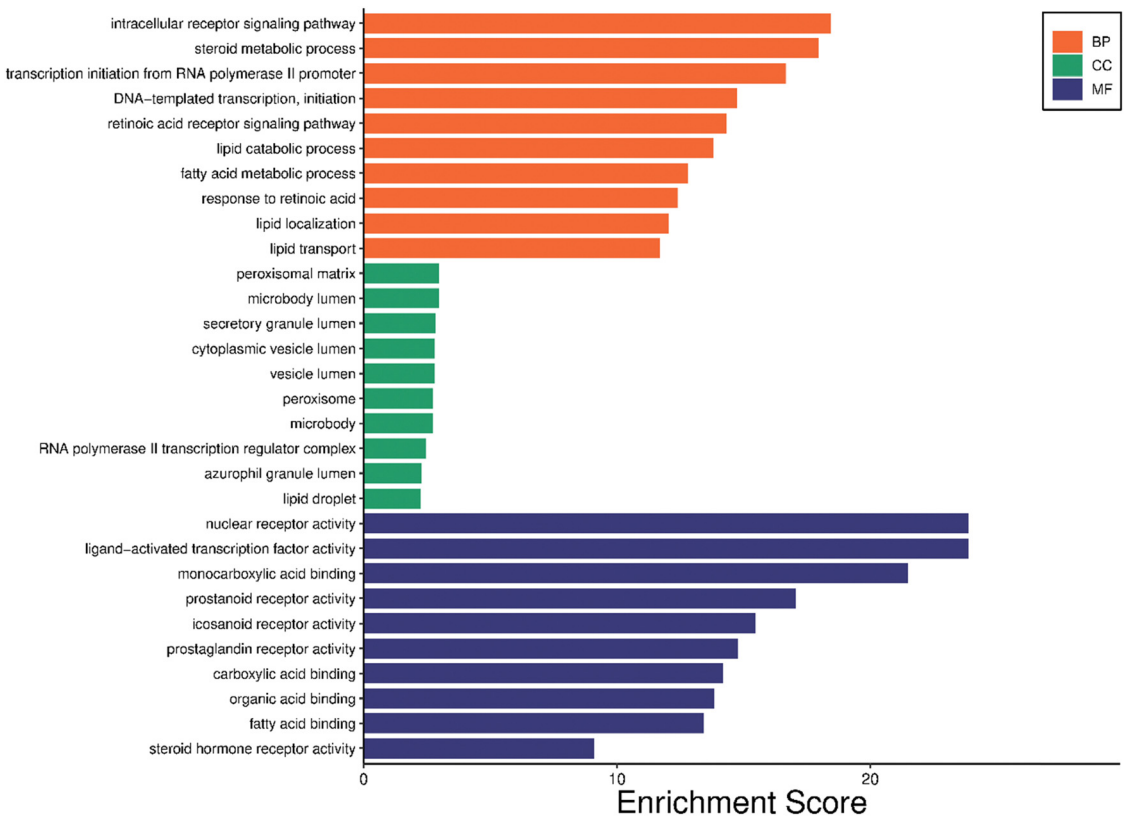

Fig. 11 Gene Ontology analysis representing the most important processes *i.e.*, BP – Biological process, MF – molecular function, and CC – cellular component) determined by the number of associated target genes as represented by *X*-axis.

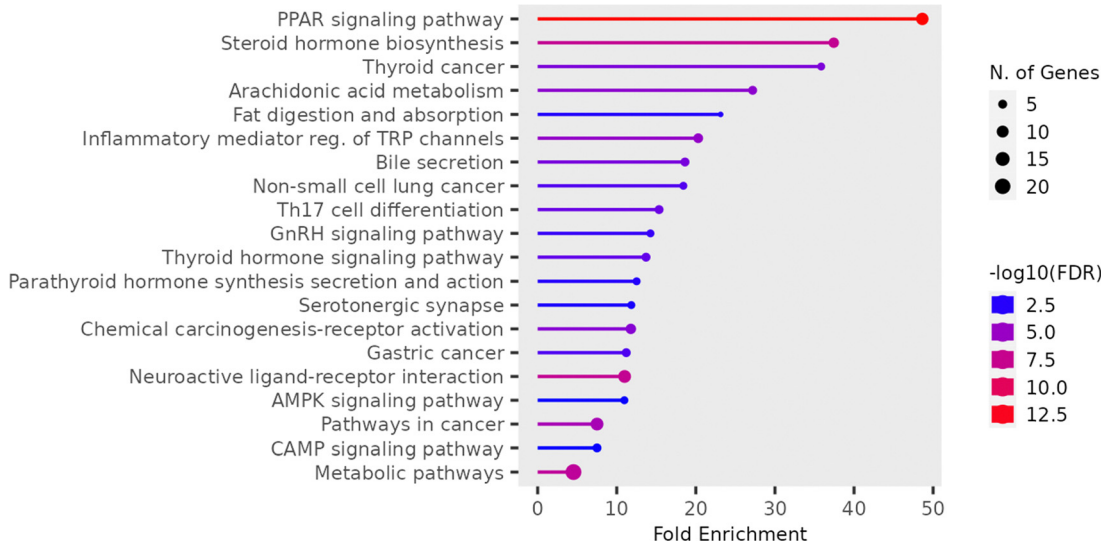

Fig. 12 Barplot for KEGG pathway enrichment analysis of top twenty target pathways.

Table 1 List of top twenty target pathways observed in pathway enrichment analysis

Enrichment FDR	nGenes	Pathway Genes	Fold Enrichment	Pathways (click for details)
6.4×10^{-14}	11	75	48.6	PPAR signalling pathway
5.0×10^{-08}	7	62	37.4	Steroid hormone biosynthesis
9.6×10^{-05}	4	37	35.8	Thyroid cancer
3.0×10^{-05}	5	61	27.2	Arachidonic acid metabolism
3.3×10^{-03}	3	43	23.1	Fat digestion and absorption
1.6×10^{-05}	6	98	20.3	Inflammatory mediator. of TRP channels
1.4×10^{-04}	5	89	18.6	Bile secretion
9.6×10^{-04}	4	72	18.4	Non-small cell lung cancer
3.2×10^{-04}	5	108	15.4	Th17 cell differentiation
2.3×10^{-03}	4	93	14.3	GnRH signaling pathway
5.1×10^{-04}	5	121	13.7	Thyroid hormone signaling pathway
3.3×10^{-03}	4	106	12.5	Parathyroid hormone synthesis secretion and action
3.8×10^{-03}	4	112	11.8	Serotonergic synapse
5.1×10^{-05}	7	197	11.8	Chemical carcinogenesis receptor activation
1.1×10^{-03}	5	148	11.2	Gastric cancer
5.0×10^{-08}	12	362	11	Neuroactive ligand-receptor interaction
4.5×10^{-03}	4	121	11	AMPK signalling pathway
2.1×10^{-06}	12	530	7.5	Pathways in cancer
4.5×10^{-03}	5	221	7.5	CAMP signalling pathway
1.2×10^{-07}	21	1538	4.5	Metabolic pathways

PPAR signalling pathway, steroid hormone biosynthesis, and arachidonic acid metabolism implicates palmitic acid in lipid metabolism and regulation of nuclear receptor activity. Additionally, the involvement of pathways related to cancer, including thyroid cancer, non-small cell lung cancer, and gastric cancer, underscores its potential significance in tumorigenesis and cancer progression. Furthermore, the enrichment of pathways such as inflammatory mediator regulation of TRP channels and serotonin synapse highlights its potential contributions to inflammatory responses and neurotransmitter signalling. Collectively, these findings provide valuable insights into the diverse biological functions and molecular mechanisms associated with palmitic acid, emphasizing its importance in physiological and pathological processes.

4. Conclusion and future perspective

The results conclude that the *T. govanianum rhizome* extract-mediated green approach for synthesizing ^{TGR}AgNPs is a simple, rapid, cost-effective, and eco-friendly method. Aqueous extracts of *T. govanianum* acted as a source of stabilizing and reducing agents for the synthesis of the silver nanoparticles. A colour change from light yellowish to dark brown was observed, implying the reduction of Ag^{+} to Ag^{0}, leading to the synthesis of silver nanoparticles. UV-vis spectrum displayed a strong absorption band at 410 nm, confirming the reduction of silver nanoparticles. Further ^{TGR}AgNPs formation was confirmed by FTIR, DLS, XRD, SEM-EDX and TEM analysis. The average particle and crystallite size was found to be 38 nm and

32 nm. SEM images displayed nanoparticles in polymorphic shapes, some irregularly granulated, ellipsoidal, and highly aggregated. The nanoparticles were found to have excellent antioxidant activity with potential cytotoxicity. Moreover, the ability of ^{TGR}AgNPs to denature bovine serum albumin suggests their anti-inflammatory potential with largely being biocompatible. Furthermore, the nanoparticles were found quite effective in protecting against free radical DNA damage. *In silico* analysis also suggest involvement of key cellular proteins and pathways, implicated in the observed biological activities of the nanoparticles, as possible targets for the anticipated palmitic acid functionalized AgNPs. Overall, the study used an economical and promising green approach for synthesizing the biocompatible and biologically active AgNPs, using rhizome extract of *Trillium govanianum.* In light of these findings, future studies in this direction should primarily focus on – (i) understanding the precise molecular mechanism of green synthesis of nanoparticles and its regulation, (ii) extensive exploration of other plant-based extracts in green nanotechnology so as to enhance the repertoire of green synthesis methods, (iii) optimization of the synthesized nanoparticle for specific use in medical field leading to the development of new therapeutics with enhanced efficiency and reduced side effects, (iv) exploration of route of administration, pharmacokinetic properties, and host immune responses, (v) advanced computational analysis to predict the behaviour of the synthesized nanoparticles under various biological environments so as to enhance its targeted applications and (vi) being environment friendly, inexpensive, simple, efficient and biocompatible, the scalability of green synthesis for large scale production should be focussed upon at the earliest. Although being very promising, challenges still remain there for achieving the uniformity and consistency in the size and shape of green synthesized nanoparticles. Future studies in this direction are also highly warranted as the scalability of green synthesis process is critical for their functioning in a specific application. In fact, addressing these challenges, through optimization and standardization of the green synthesis process, is crucial for large-scale implementation of the green nanotechnology.

Author contributions

SIM – Data curation, formal analysis, methodology, writing – original draft; FJ – methodology, data curation; RJ – formal analysis, conceptualization; MAR – manuscript reading, KI – data curation, data analysis, methodology; MAM – conceptualization, data curation, software, formal analysis, writing – original draft, supervision, investigation; TAD – conceptualization, data curation, formal analysis, writing – original draft, supervision, investigation, revision of the manuscript.

Informed consent

Due informed consent was obtained for experimentation with human subjects.

Data availability

There is no such repository or link that can be generated for the availability of data. However, the raw data generated is available on the lab instruments and will be available upon request.

Conflicts of interest

The authors declare that there is no conflict of interest.

Acknowledgements

This work was supported by the grant provided by Central Council for Research in Unani Medicine, Govt. of India, New Delhi to TAD with grant number: F. No. 3-67/2022-CCRUM/Tech.

References

1 S. Modi, R. Prajapati, G. K. Inwati, N. Deepa, V. Tirth, V. K. Yadav and B. H. Jeon, Recent trends in fascinating applications of nanotechnology in allied health sciences, *Crystals*, 2021, **12**(1), 39.
2 R. Tian, M. Li, H. Teng, H. Luo, D. Yan and D. M. Wei, Surface enhanced Raman scattering based on Au nanoparticles/layered double hydroxide ultrathin films, *J. Mater. Chem.*, 2015, **3**(20), 5167–5174.
3 A. K. Keshari, R. Srivastava, P. Singh, V. B. Yadav and G. Nath, Antioxidant and antibacterial activity of silver nanoparticles synthesized by Cestrum nocturnum, *J. Ayurveda Integr. Med.*, 2020, **11**(1), 37–44.
4 R. Tian, S. Zhang, M. Li, Y. Zhou, B. Lu, D. Yan and X. Duan, Localization of Au nanoclusters on layered double hydroxides nanosheets: confinement-induced emission enhancement and temperature-responsive luminescence, *Adv. Funct. Mater.*, 2015, **25**(31), 5006–5015.
5 M. A. Sofi, S. Sunitha, S. K. Pasha and D. Choi, An overview of antimicrobial and anticancer potential of silver nanoparticles, *J. King Saud Univ., Sci.*, 2022, **34**(2), 101791.
6 T. Zhang, H. Shang, B. Zhang, D. Yan and X. Xiang, Ag/ultrathin-layered double hydroxide nanosheets induced by a self-redox strategy for highly selective CO2 reduction, *ACS Appl. Mater. Interfaces*, 2021, **13**(14), 16536–16544.
7 S. Wei, Y. Wang, Z. Tang, H. Xu, Z. Wang, T. Yang and T. Zou, A novel green synthesis of silver nanoparticles by the residues of Chinese herbal medicine and their biological activities, *RSC Adv.*, 2021, **11**(3), 1411–1419.
8 A. Dhaka, S. C. Mali and S. Sharma, Trivedi, A review on biological synthesis of silver nanoparticles and their potential applications, *Results Chem.*, 2023, 101108.
9 P. K. Dikshit, J. Kumar, A. K. Das, S. Sadhu, S. Sharma, S. Singh, P. K. gupta and S. Kim, Green synthesis of metallic nanoparticles: Applications and limitations, *Catalysts*, 2021, **11**(8), 902.
10 M. Tariq, K. N. Mohammad, B. Ahmed, M. A. Siddiqui and J. Lee, Biological synthesis of silver nanoparticles and

prospects in plant disease management, *Molecules*, 2022, **27**(15), 4754.
11 S. Simon, N. R. Sibuyi, A. O. Fadaka, S. Meyer, J. Josephs, M. O. Onani and A. M. Madiehe, Biomedical applications of plant extract-synthesized silver nanoparticles, *Biomedicines*, 2022, **10**(11), 2792.
12 M. A. Kakakhel, W. Sajjad, F. Wu, N. Bibi, K. Shah, Z. Yali and W. Wang, Green synthesis of silver nanoparticles and their shortcomings, animal blood a potential source for silver nanoparticles: A review, *J. Hazard. Mater. Adv.*, 2021, **1**, 100005.
13 A. K. Sidhu, N. Verma and P. Kaushal, Role of biogenic capping agents in the synthesis of metallic nanoparticles and evaluation of their therapeutic potential, *Front. Nanotechnol.*, 2022, **3**, 801620.
14 A. Rozhin, S. Batasheva, M. Kruychkova, Y. Cherednichenko, E. Rozhina and R. Fakhrullin, Biogenic silver nanoparticles: Synthesis and application as antibacterial and antifungal agents, *Micromachines*, 2021, **12**(12), 1480.
15 D. Kulkarni, R. Sherkar, C. Shirsathe, R. Sonwane, N. Varpe, S. Shelke and S. Dyawanapelly, Biofabrication of nanoparticles: sources, synthesis, and biomedical applications, *Front. Bioeng. Biotechnol.*, 2023, **11**, 1159193.
16 P. Saha, M. Mahiuddin, A. N. Islam and B. Ochiai, Biogenic synthesis and catalytic efficacy of silver nanoparticles based on peel extracts of citrus macroptera fruit, *ACS Omega*, 2021, **6**(28), 18260–18268.
17 A. K. Alzubaidi, W. J. Al-Kaabi, A. A. Ali, S. Albukhaty, H. Al-Karagoly, G. M. Sulaiman and Y. Khane, Green synthesis and characterization of silver nanoparticles using flaxseed extract and evaluation of their antibacterial and antioxidant activities, *Appl. Sci.*, 2023, **13**(4), 2182.
18 K. D. Dejen, D. Y. Kibret, T. H. Mengesha, E. T. Bekele, A. Tedla, T. A. Bafa and F. T. Derib, Green synthesis and characterisation of silver nanoparticles from leaf and bark extract of Croton macrostachyus for antibacterial activity, *Mater. Technol.*, 2023, **38**(1), 2164647.
19 A. K. Giri, B. Jena, B. Biswal, A. K. Pradhan, M. Arakha and S. Acharya, Green synthesis and characterization of silver nanoparticles using Eugenia roxburghii DC. extract and activity against biofilm-producing bacteria, *Sci. Rep.*, 2022, **12**(1), 8383.
20 H. B. Habeeb Rahuman, R. Dhandapani, S. Narayanan, V. Palanivel, R. Paramasivam, R. Subbarayalu and S. Muthupandian, Medicinal plants mediated the green synthesis of silver nanoparticles and their biomedical applications, *IET Nanobiotechnol.*, 2022, **16**(4), 115–144.
21 B. Essghaier, H. Hannachi, R. Nouir, F. Mottola and L. Rocco, Green Synthesis and characterization of Novel Silver nanoparticles using Achillea maritima subsp. maritima Aqueous Extract: antioxidant and antidiabetic potential and effect on virulence mechanisms of bacterial and fungal pathogens, *Nanomaterials*, 2023, **13**, 1964.
22 R. S. Patil, M. R. Kokate and S. S. Kolekar, Bioinspired synthesis of highly stabilized silver nanoparticles using Ocimum tenuiflorssum leaf extract and their antibacterial activity, *Spectrochim. Acta, Part A*, 2012, **91**, 234–238.
23 R. K. Omole, R. C. George, O. I. Adeyemi, N. Torimiro, M. Saravanan, E. O. Agboluaje and M. P. Xiong, Spectral Characterization of Silver Nanoparticles Biosynthesized from Lysinibacillus fusiformis and its Antibacterial Efficacy Against Multidrug-Resistant Bacteria Isolated from Chronic Wounds, *Bionanoscience*, 2024, 1–11.
24 U. P. Manik, A. Nande, S. Raut and S. J. Dhoble, Green synthesis of silver nanoparticles using plant leaf extraction of Artocarpus heterophylus and Azadirachta indica, *Results Mater.*, 2020, **6**, 100086.
25 A. Maniraj, M. Kannan, K. Rajarathinam, S. Vivekanandhan and S. Muthuramkumar, Green synthesis of silver nanoparticles and their effective utilization in fabricating functional surface for antibacterial activity against multi-drug-resistant Proteus mirabilis, *J. Cluster Sci.*, 2019, **30**, 1403–1414.
26 S. Priyadarshini, S. Sulava, R. Bhol and S. Jena, Green synthesis of silver nanoparticles using Azadirachta indica and Ocimum sanctum leaf extract, *Curr. Sci.*, 2019, **117**(8), 1300–1307.
27 A. Mathesh, D. S. Carmelin, A. Mohanprasanth, P. Geetha Sravanthy, R. Snega, M. Surya and M. Saravanan, Tridax procumbens–mediated one pot synthesis of silver-doped fucoidan nanoparticles and their antibacterial, antioxidant, and anti-inflammatory efficacy, *Biomass Convers. Biorefin.*, 2024, **14**(8), 9887–9896.
28 R. Manikandan, M. Beulaja, N. M. Prabhu, R. Thiagarajan, M. Anjugam, S. Palanisamy, K. Saravanan and M. Arumugam, Synthesis of silver nanoparticles using Solanum trilobatum fruits extract and its antibacterial, cytotoxic activity against human breast cancer cell line MCF 7, *Spectrochim. Acta, Part A*, 2015, **140**, 223–228.
29 G. Kuppurangan, B. Karuppasamy, K. Nagarajan, K. S. Rajkumar, V. Nilmini and R. Thirumurugan, Biogenic synthesis and spectroscopic characterization of silver nanoparticles using leaf extract of Indoneesiella echioides: in vitro assessment on antioxidant, antimicrobial and cytotoxicity potential, *Appl. Nanosci.*, 2016, **6**(7), 973–982.
30 P. Kannaiyan, Greener approach for synthesis of antibacterial silver nanoparticles using aqueous solution of neem gum (Azadirachta indica L.), *Ind. Crops Prod.*, 2015, **66**, 103–109.
31 M. Ramar, B. Manikandan, P. N. Marimuthu, T. Raman, A. Mahalingam, P. Subramanian and A. Munusamy, Silver nanoparticles biosynthesized using Achillea biebersteinii flower extract: apoptosis induction in MCF-7 cells via caspase activation and regulation of Bax and Bcl-2 gene expression, *Molecules*, 2015, **20**(2), 2693–2706.
32 T. M. Abdelghany, A. M. Al-Rajhi, M. A. Al Abboud, M. M. Alawlaqi, A. Ganash Magdah, E. A. Helmy and A. S. Mabrouk, Recent advances in green synthesis of silver nanoparticles and their applications: about future directions, A review, *Bionanoscience*, 2018, **8**, 5–16.
33 R. Verma, A. Tapwal, D. Kumar and S. Puri, Antimicrobial potential and phytochemical profiling of ethnomedicinal plant Trillium govanianum Wall. ex D. Don in Western Himalaya, *J. Herb. Med.*, 2021, **29**, 100491.

34 K. Uz-Zaman, J. Bakht, B. K. Malikovna, E. R. Elsharkawy, A. A. Khalil, S. Bawazeer and A. Rauf, Trillium govanianum Wall. Ex. Royle rhizomes extract-medicated silver nanoparticles and their antimicrobial activity, *Green Process. Synth.*, 2020, **9**, 503–514.
35 Z. Bedlovicova, I. Strapac, M. Balaz and A. Salayova, A brief overview on antioxidant activity determination of silver nanoparticles, *Molecules*, 2020, **25**(14), 3191.
36 S. Andleeb, F. Tariq, A. Muneer, T. Nazir, B. Shahid, Z. Latif and D. A. Al Farraj, In vitro bactericidal, antidiabetic, cytotoxic, anticoagulant, and hemolytic effect of green-synthesized silver nanoparticles using Allium sativum clove extract incubated at various temperatures, *Green Process. Synth.*, 2020, **9**(1), 538–553.
37 K. Imtiyaz, A. Husain Rahmani, M. A. Alsahli, S. A. Almatroodi and M. M. A. Rizvi, Fisetin induces apoptosis in human skin cancer cells through downregulating MTH1, *J. Biomol. Struct. Dyn.*, 2023, **4**(15), 7339–7353.
38 A. Algarni, A. Fayomi, H. A. Garalleh and A. Afand, Nanofabrication synthesis and its role in antibacterial, anti-inflammatory, and anticoagulant activities of AgNPs synthesized by Mangifera indica bark extract, *Environ. Res.*, 2023, **231**, 115983.
39 X. Wu and S. Dhanasekaran, Protective effect of leaf extract of Abutilon indicum on DNA damage and peripheral blood lymphocytes in combating the oxidative stress, *Saudi Pharm. J.*, 2020, **28**(8), 943.
40 R. Pluskota, K. Jaroch, P. Kośliński, B. Ziomkowska, A. Lewińska, S. Kruszewski and M. Koba, Selected drug-likeness properties of 2-arylidene-indan-1, 3-dione derivatives—chemical compounds with potential anti-cancer activity, *Molecules*, 2021, **26**(17), 5256.
41 X. Wang, Y. Shen, S. Wang, S. Li, W. Zhang, X. Liu and H. Li, PharmMapper 2017 update: a web server for potential drug target identification with a comprehensive target pharmacophore database, *Nucleic Acids Res.*, 2017, **45**, W356–W360.
42 C. Mu, Y. Sheng, Q. Wang, A. Amin, X. Li and Y. Xie, Potential compound from herbal food of Rhizoma Polygonati for treatment of COVID-19 analyzed by network pharmacology: Viral and cancer signaling mechanisms, *J. Funct. Foods*, 2021, **77**, 104149.
43 C. Li, Z. Gao, B. Su, G. Xu and X. Lin, Data analysis methods for defining biomarkers from omics data, *Anal. Bioanal. Chem.*, 2022, **414**(1), 235–250.
44 M. R. Karim, M. N. Morshed, S. Iqbal, S. Mohammad, R. Mathiyalagan, D. C. Yang and D. U. Yang, A Network Pharmacology and Molecular-Docking-Based Approach to Identify the Probable Targets of Short-Chain Fatty-Acid-Producing Microbial Metabolites against Kidney Cancer and Inflammation, *Biomolecules*, 2023, **13**(11), 1678.
45 L. Lv, X. Wang and H. Wu, Assessment of palmitic acid toxicity to animal hearts and other major organs based on acute toxicity, network pharmacology, and molecular docking, *Comput. Biol. Med.*, 2017, **158**, 106899.
46 J. Peng, H. Wang, J. Lu, W. Hui, Y. Wang and X. Shang, Identifying term relations cross different gene ontology categories, *BMC Bioinf.*, 2017, **18**, 67–74.
47 M. A. Malik, A. A. Alshehri and R. Patel, Facile one-pot green synthesis of Ag–Fe bimetallic nanoparticles and their catalytic capability for 4-nitrophenol reduction, *J. Mater. Res. Technol.*, 2021, **12**, 455–470.
48 A. Chhatre, P. Solasa, S. Sakle, R. Thaokar and A. Mehra, Color and surface plasmon effects in nanoparticle systems: Case of silver nanoparticles prepared by microemulsion route, *Colloids Surf., A*, 2012, **404**, 83–92.
49 B. Bharath, K. Perinbam, S. Devanesan, M. S. AlSalhi and M. Saravanan, Evaluation of the anticancer potential of Hexadecanoic acid from brown algae Turbinaria ornata on HT–29 colon cancer cells, *J. Mol. Struct.*, 2021, **1235**, 130229.
50 Q. Gan, J. Wang, J. Hu, G. Lou, H. Xiong, C. Peng and Q. Huang, The role of diosgenin in diabetes and diabetic complications, The, *J. Steroid Biochem. Mol. Biol.*, 2020, **198**, 105575.
51 K. Kogure, Novel antioxidative activity of astaxanthin and its synergistic effect with vitamin E, *J. Nutr. Sci. Vitaminol.*, 2019, **65**, S109–S112.
52 K. M. Khan, S. D. Sarker, G. A. Khan, H. Saleem, S. A. Khan and A. Mannan, Phytochemical profiling and evaluation of modified resazurin microtiter plate assay of the roots of Trillium govanianum, *Nat. Prod. Res.*, 2020, **34**(19), 2837–2841.
53 K. S. Siddiqi, A. Husen and R. A. Rao, A review on biosynthesis of silver nanoparticles and their biocidal properties, *J. Nanobiotechnol.*, 2018, **16**, 1–28.
54 S. U. R. Qamar and J. N. Ahmad, Nanoparticles, Mechanism of biosynthesis using plant extracts, bacteria, fungi, and their applications, *J. Mol. Liq.*, 2021, **334**, 116040.
55 K. Rashid, S. Rashid, A. H. Ganie and I. A. Nawchoo, Trillium govanianum–A Promising Endemic Medicinal Herb of the Himalaya, *Bioprospecting of Tropical Medicinal Plants.*, 2023, 381–408.
56 S. Mukherji, S. Bharti and G. Shukla, Mukherji, Synthesis and characterization of size-and shape-controlled silver nanoparticles, *Phys. Sci. Rev.*, 2018, **4**(1), 20170082.
57 M. A. Ansari, S. M. M. Asiri, M. A. Alzohairy, M. N. Alomary, A. Almatroudi and F. A. Khan, Biofabricated fatty acids-capped silver nanoparticles as potential antibacterial, antifungal, antibiofilm and anticancer agents, *Pharmaceuticals*, 2021, **14**(2), 139.
58 J. A. Hema, R. Malaka, N. P. Muthukumarasamy, A. Sambandam, S. Subramanian and M. Sevanan, Green synthesis of silver nanoparticles using Zea mays and exploration of its biological applications, *IET Nanobiotechnol.*, 2016, **10**(5), 288–294.
59 M. H. Ali, M. A. Azad, K. A. Khan, M. O. Rahman, U. Chakma and A. Kumer, Analysis of crystallographic structures and properties of silver nanoparticles synthesized using PKL extract and nanoscale characterization techniques, *ACS Omega*, 2023, **8**, 28133–28142.

60 A. A. Alshehri and M. A. Malik, Phytomediated photo-induced green synthesis of silver nanoparticles using Matricaria chamomilla L. and its catalytic activity against rhodamine B, *Biomolecules*, 2020, **10**, 1604.
61 S. S. Albeladi, M. A. Malik and S. A. Al-thabaiti, Facile Preparation of Ag Flower-Like Nanostructures and Their Catalytic Properties in the Degradation of Organic Dyes, *J. Mater. Res. Technol.*, 2020, **9**, 10031.
62 M. Stevanovic, I. Savanović, V. Uskoković, S. D. Škapin, I. Bračko, U. Jovanović and D. Uskoković, A new, simple, green, and one-pot four-component synthesis of bare and poly (α, γ, L-glutamic acid)-capped silver nanoparticles, *Colloid Polym. Sci.*, 2012, **290**, 221–231.
63 S. Singla, A. Jana, R. Thakur, C. Kumari and S. Goyal, Pradhan, Antioxidants and antibacterial potential of extracts of seed of Quercus leucotrichophora A. camus, *Curr. Res. Green Sustainable Chem.*, 2023, **7**, 100375.
64 K. Saware and A. Venkataraman, Biosynthesis and characterization of stable silver nanoparticles using Ficus religiosa leaf extract: a mechanism perspective, *J. Cluster Sci.*, 2014, **25**, 1157–1171.
65 R. G. Saratale, G. Benelli, G. Kumar, D. S. Kim and E. D. Saratale, Bio-fabrication of silver nanoparticles using the leaf extract of ancient herbal medicine, dandelion (Taraxacum officinale), evaluation of their antioxidant, anticancer potential, and antimicrobial activity against phytopathogens, *Environ. Sci. Pollut. Res.*, 2018, **25**, 10392–10406.
66 S. Some, O. Bulut and K. Biswas, *et al.*, Effect of feed supplementation with biosynthesized silver nanoparticles using leaf extract of Morus indica L. V1 on Bombyx mori L. (Lepidoptera: Bombycidae), *Sci. Rep.*, 2019, **9**(1), 14839.
67 S. Peron, F. Hadi, F. Azarbani and H. C. Ananda Murthy, Antimicrobial, antioxidant, anti-glycation and toxicity studies on silver nanoparticles synthesized using Rosa damascena flower extract, *Green Chem. Lett. Rev.*, 2021, **14**(3), 519–533.
68 T. Desalegn, C. R. Ravikumar and H. C. A. Murthy, Eco-friendly synthesis of silver nanostructures using medicinal plant Vernonia amygdalina Del. leaf extract for multifunctional applications, *Appl. Nanosci.*, 2021, **11**, 535–551.
69 D. Kumar and V. Kumari, Metabolite profiling, antidiabetic, and antioxidant potential of different tissues of Trillium govanianum Wall. ex D. Don, *S. Afr. J. Bot.*, 2023, **153**, 102–108.
70 A. K. Sidhu, N. Verma and P. Kaushal, Role of biogenic capping agents in the synthesis of metallic nanoparticles and evaluation of their therapeutic potential, *Front. Nanotechnol.*, 2022, **3**, 801620.
71 S. Baliyan, R. Mukherjee, A. Priyadarshini, A. Vibhuti, A. Gupta, R. P. Pandey and C. M. Chang, Determination of antioxidants by DPPH radical scavenging activity and quantitative phytochemical analysis of Ficus religiosa, *Molecules*, 2022, **27**(4), 1326.
72 S. R. Guntur, N. S. Kumar, M. M. Hegde and V. R. Dirisala, In vitro studies of the antimicrobial and free-radical scavenging potentials of silver nanoparticles biosynthesized from the extract of Desmostachya bipinnata, *Anal. Chem. Insights*, 2018, **13**, 1177390118782877.
73 J. Singh and A. S. Dhaliwal, Novel green synthesis and characterization of the antioxidant activity of silver nanoparticles prepared from Nepeta leucophylla root extract, *Anal. Lett.*, 2019, **52**(2), 213–230.
74 M. S. Abdel-Aziz, M. S. Shaheen, A. A. El-Nekeety and M. A. Abdel-Wahhab, Antioxidant and antibacterial activity of silver nanoparticles biosynthesized using Chenopodium murale leaf extract, *J. Saudi Chem. Soc.*, 2014, **18**(4), 356–363.
75 M. Sharifi-Rad, P. Pohl, F. Epifano and J. M. Álvarez-Suarez, Green synthesis of silver nanoparticles using Astragalus tribuloides delile root extract, Characterization, antioxidant, antibacterial, and anti-inflammatory activities, *Nanomaterials*, 2020, **10**(12), 2383.
76 S. N. Kharat and V. D. Mendhulkar, Synthesis, characterization and studies on antioxidant activity of silver nanoparticles using Elephantopus scaber leaf extract, *Mater. Sci. Eng., C*, 2016, **62**, 719–724.
77 M. Mousavi-Khattat, M. Keyhanfar and A. Razmjou, A comparative study of stability, antioxidant, DNA cleavage and antibacterial activities of green and chemically synthesized silver nanoparticles, *Artif. Cells, Nanomed., Biotechnol.*, 2018, **46**(3), 1022–1031.
78 S. E. Arland and J. Kumar, Green and chemical syntheses of silver nanoparticles: Comparative and comprehensive study on characterization, therapeutic potential, and cytotoxicity, *Eur. J. Med. Chem. Rep.*, 2024, **11**, 100168.
79 S. Suman, L. Loveleen, M. Bhandari, A. Syed, A. H. Bahkali, R. Manchanda and S. Nimesh, Antibacterial, antioxidant, and haemolytic potential of silver nanoparticles biosynthesized using roots extract of Cannabis sativa plant, *Artif. Cells, Nanomed., Biotechnol.*, 2022, **50**(1), 343–351.
80 E. Parthiban, N. Manivannan, R. Ramanibai and N. Mathivanan, Green synthesis of silver-nanoparticles from Annona reticulata leaves aqueous extract and its mosquito larvicidal and anti-microbial activity on human pathogens, *Biotechnol. Rep.*, 2019, **21**, e00297.
81 A. Mishra, N. K. Kaushik, M. Sardar and D. Sahal, Evaluation of antiplasmodial activity of green synthesized silver nanoparticles, *Colloids Surf., B*, 2013, **111**, 713–718.
82 Y. Bian, K. Kim, T. Ngo, I. Kim, O. N. Bae, K. M. Lim and J. H. Chung, Silver nanoparticles promote procoagulant activity of red blood cells: a potential risk of thrombosis in susceptible population, *Part. Fibre Toxicol.*, 2019, **16**, 1–14.
83 B. M. Rothen, S. Schürch, B. Haenni, N. Kapp and P. Gehr, Interaction of fine particles and nanoparticles with red blood cells visualized with advanced microscopic techniques, *Environ. Sci. Technol.*, 2006, **40**(14), 4353–4359.
84 P. Kuppusamy, S. J. Ichwan, P. N. Al-Zikri, W. H. Suriyah, I. Soundharrajan, N. Govindan and M. M. Yusoff, In vitro anticancer activity of Au, Ag nanoparticles synthesized using Commelina nudiflora L. aqueous extract against

HCT-116 colon cancer cells, *Biol. Trace Elem. Res.*, 2016, **173**, 297–305.

85 M. Madakka, N. Jayaraju and N. Rajesh, Evaluating the antimicrobial activity and antitumor screening of green synthesized silver nanoparticles compounds, using Syzygium jambolanum, towards MCF7 cell line (Breast cancer cell line), *J. Photochem. Photobiol.*, 2021, **6**, 100028.

86 D. Acharya, S. Satapathy, P. Somu, U. K. Parida and G. Mishra, Apoptotic effect and anticancer activity of biosynthesized silver nanoparticles from marine algae Chaetomorpha linum extract against human colon cancer cell HCT-116, *Biol. Trace Elem. Res.*, 2013, **199**(5), 1812–1822.

87 A. Balkrishna, V. K. Sharma, S. K. Das, N. Mishra, L. Bisht, A. Joshi and N. Sharma, Characterization and anticancerous effect of Putranjiva roxburghii seed extract mediated silver nanoparticles on human colon (HCT-116), pancreatic (PANC-1) and breast (MDA-MB 231) cancer cell lines: A comparative study, *Int. J. Nanomed.*, 2020, 573–585.

88 S. Tian, K. Saravanan, R. A. Mothana, G. Ramachandran, G. Rajivgandhi and N. Manoharan, Anti-cancer activity of biosynthesized silver nanoparticles using Avicennia marina against A549 lung cancer cells through ROS/mitochondrial damages, *Saudi J. Biol. Sci.*, 2020, **27**(11), 3018–3024.

89 S. Kummara, M. B. Patil and T. Uriah, Synthesis, characterization, biocompatible and anticancer activity of green and chemically synthesized silver nanoparticles–a comparative study, *Biomed. Pharmacother.*, 2016, **84**, 10–21.

90 R. Amooaghaie, M. R. Saeri and M. Azizi, Synthesis, characterization and biocompatibility of silver nanoparticles synthesized from Nigella sativa leaf extract in comparison with chemical silver nanoparticles, *Ecotoxicol. Environ. Saf.*, 2015, **120**, 400–408.

91 F. B. Almukaynizi, M. H. Daghestani, M. A. Awad, A. Althomali, N. M. Merghani, W. I. Bukhari and R. S. Bhat, Cytotoxicity of green-synthesized silver nanoparticles by Adansonia digitata fruit extract against HTC116 and SW480 human colon cancer cell lines, *Green Process. Synth.*, 2022, **11**(1), 411–422.

92 F. Yousefbeyk, S. Dabirian, S. Ghanbarzadeh, D. Eghbali Koohi, P. Yazdizadeh and S. Ghasemi, Green synthesis of silver nanoparticles from Stachys byzantina K. Koch: characterization, antioxidant, antibacterial, and cytotoxic activity, *Part. Sci. Technol.*, 2022, **40**(2), 219–232.

93 S. U. Rahman, M. Ismail, M. R. Shah, M. Iriti and M. Shahid, GC/MS analysis, free radical scavenging, anticancer and β-glucuronidase inhibitory activities of Trillium govanianum rhizome, *Bangladesh J. Pharmacol.*, 2015, **10**(3), 577–583.

94 X. Wang, C. Zhang and N. Bao, Molecular mechanism of palmitic acid and its derivatives in tumor progression, *Front. Oncol.*, 2023, **13**, 1224125.

95 G. Sangeetha and R. Vidhya, In vitro anti-inflammatory activity of different parts of Pedalium murex (L.), *Inflammation*, 2016, **4**(3), 31–36.

96 M. Sharifi-Rad, P. Pohl, F. Epifano and J. M. Álvarez-Suarez, Green synthesis of silver nanoparticles using Astragalus tribuloides delile root extract: Characterization, antioxidant, antibacterial, and anti-inflammatory activities, *Nanomaterials*, 2020, **10**(12), 2383.

97 F. S. Alatawi, M. S. Alatawi, A. M. Omran, R. M. Jame, M. Adnan, M. N. Khan and M. Rahimi, Aconitum lycoctonum L. (Ranunculaceae) mediated biogenic synthesis of silver nanoparticles as potential antioxidant, anti-inflammatory, antimicrobial and antidiabetic agents, *BMC Chem.*, 2023, **17**(1), 128.

98 P. B. E. Kedi, C. C. Nanga, A. P. Gbambie, V. Deli, F. E. A. Meva, H. E. A. Mohamed and M. H. J. Nkors, Biosynthesis of silver nanoparticles from Microsorum punctatum (l.) copel fronds extract and an in-vitro anti-inflammation study, *J. Nanotechnol. Res.*, 2020, **2**(2), 25–41.

99 M. B. Lava, U. M. Muddapur, N. Basavegowda, S. S. More and V. S. More, Characterization, anticancer, antibacterial, anti-diabetic and anti-inflammatory activities of green synthesized silver nanoparticles using Justica wynaadensis leaves extract, *Mater. Today: Proc.*, 2021, **46**, 5942–5947.

100 P. Salve, A. Vinchurkar, R. Raut, R. Chondekar, J. Lakkakula, A. Roy and M. F. Nur Azlina, an evaluation of antimicrobial, anticancer, anti-inflammatory and antioxidant activities of silver nanoparticles synthesized from leaf extract of Madhuca longifolia utilizing quantitative and qualitative methods, *Molecules*, 2022, **27**(19), 6404.

101 S. Ur Rahman, A. Adhikari, M. Ismail, M. Raza Shah, M. Khurram, M. Shahid and M. Iriti, Beneficial effects of Trillium govanianum rhizomes in pain and inflammation, *Molecules*, 2016, **21**(8), 1095.

102 Z. U. R. Khan, N. Assad, M. Naeem-ul-Hassan, M. Sher, F. S. Alatawi, M. S. Alatawi and M. Rahimi, Aconitum lycoctonum L. (Ranunculaceae) mediated biogenic synthesis of silver nanoparticles as potential antioxidant, anti-inflammatory, antimicrobial and antidiabetic agents, *BMC Chem.*, 2023, **17**(1), 128.

103 T. Gur, Green synthesis, characterizations of silver nanoparticles using sumac (Rhus coriaria L.) plant extract and their antimicrobial and DNA damage protective effects, *Front. Chem.*, 2022, **10**, 968280.

104 J. Singh and A. S. Dhaliwal, Novel green synthesis and characterization of the antioxidant activity of silver nanoparticles prepared from Nepeta leucophylla root extract, *Anal. Lett.*, 2019, **52**(2), 213–230.

105 A. S. Shinde and V. D. Mendhulkar, Antiproliferative activity of Elephantopus scaber mediated silver nanoparticles against MCF-7, A-549, SCC-40 and COLO-205 human cancer cell lines, *Asian J. Pharm. Clin. Res.*, 2020, **13**(2), 163–167.

106 F. Sharifi, F. Sharififar, S. Soltanian, M. Doostmohammadi and N. Mohamadi, Synthesis of silver nanoparticles using Salvia officinalis extract: Structural characterization, cytotoxicity, antileishmanial and antimicrobial activity, *Nanomed. Res. J.*, 2020, **5**(4), 339–346.

107 J. Baharara, T. Ramezani, M. Mousavi and M. Asadi-Samani, Antioxidant and anti-inflammatory activity of green synthesized silver nanoparticles using Salvia officinalis extract, *Ann. Trop Med Int Health*, 2017, **10**(5), 1265–1270.

108 M. Kumara Swamy, K. M. Sudipta, K. Jayanta and S. Balasubramanya, The green synthesis, characterization, and evaluation of the biological activities of silver nanoparticles synthesized from Leptadenia reticulata leaf extract, *Appl. Nanosci.*, 2015, **5**, 73–81.

109 N. S. Kumaran, In vitro anti-inflammatory activity of silver nanoparticle synthesized Avicennia marina (Forssk.) Vierh.: A green synthetic approach, *Int. J. Green Pharm.*, 2018, **12**(3), 528–536.

110 O. Hotan, A. Alhaj, A. Al-quhaim, K. Alburaihi, Y. Ahmed, Q. Munasser and M. Almoiliqy, Evaluating the pharmacological activities of Aloe perryi–Silver nanoparticles induced apoptosis against colon cancer cells (HCT-116), *Food Sci. Nutr.*, 2024, **12**(8), 5890–5906.

111 D. Ayodhya, A. Ambala, G. Balraj, M. P. Kumar and P. Shyam, Green synthesis of CeO2 NPs using Manilkara zapota fruit peel extract for photocatalytic treatment of pollutants, antimicrobial, and antidiabetic activities, *Results Chem.*, 2022, **4**, 100441.

112 P. Moteriya and S. Chanda, Biosynthesis of silver nanoparticles formation from Caesalpinia pulcherrima stem metabolites and their broad spectrum biological activities, *J. Genet. Eng. Biotechnol.*, 2018, **16**(1), 105–113.

113 H. S. Hussein, C. Ngugi, F. M. Tolo and E. N. Maina, Anticancer potential of silver nanoparticles biosynthesized using Catharanthus roseus leaves extract on cervical (HeLa229) cancer cell line, *Sci. Afr.*, 2024, e02268.

114 H. S. Al-Shmgani, W. H. Mohammed, G. M. Sulaiman and A. H. Saadoon, Biosynthesis of silver nanoparticles from Catharanthus roseus leaf extract and assessing their antioxidant, antimicrobial, and wound-healing activities, *Artif. Cells, Nanomed., Biotechnol.*, 2017, **45**(6), 1234–1240.

115 J. A. Badmus, S. A. Oyemomi, O. T. Adedosu, T. A. Yekeen, M. A. Azeez, E. A. Adebayo and J. L. Marnewick, Photo-assisted bio-fabrication of silver nanoparticles using Annona muricata leaf extract: exploring the antioxidant, anti-diabetic, antimicrobial, and cytotoxic activities, *Heliyon*, 2020, **6**(11), 1–9.

116 J. A. Badmus, S. A. Oyemomi, J. O. Fatoki, T. A. Yekeen, O. T. Adedosu, P. I. Adegbola and A. Lateef, Anti-haemolytic and cytogenotoxic potential of aqueous leaf extract of Annona muricata (L.) and its bio-fabricated silver nanoparticles, *Caryologia*, 2022, **75**(1), 3–13.

117 M. Z. Gharari, S. Sadighian, A. Yazdinezhad and A. Sharafi, Green Synthesized Silver Nanostructure Using Rhus coriaria Fruit Extract Inhibits the Growth of Malignant MCF-7 Cell Line, *Braz. Arch. Biol. Technol.*, 2021, **64**, e21210069.

118 F. Pifferi, B. Laurent and M. Plourde, Lipid transport and metabolism at the blood-brain interface: Implications in health and disease, *Front. Physiol.*, 2021, **12**, 645646.

119 H. T. Yao, Y. W. Chang, S. J. Lan, C. T. Chen, J. T. Hsu and T. K. Yeh, The inhibitory effect of polyunsaturated fatty acids on human CYP enzymes, *Life Sci.*, 2006, **79**(26), 2432–2440.